

New results for the two neutrino double beta decay in deformed nuclei with angular momentum projected basis

A. A. Raduta^{a),b)}, C. M. Raduta^{b)}, A. Escuderos^{c),d)}

^{a)}*Department of Theoretical Physics and Mathematics,
Bucharest University, POBox MG11, Romania*

^{b)}*Institute of Physics and Nuclear Engineering, Bucharest, POBox MG6, Romania*

^{c)}*Instituto de Estructura de la Materia,
Consejo Superior de Investigaciones Cientificas,
Serrano 123, E-28006 Madrid, Spain and*

^{d)}*Department of Physics and Astronomy, Rutgers University,
Piscataway, New Jersey USA 08854-8019*

Abstract

Using an angular momentum projected single particle basis, a pnQRPA approach is used to study the $2\nu\beta\beta$ properties of ten isotopes, exhibiting various quadrupole deformations. The mother and daughter nuclei exhibit different quadrupole deformations. Since the projected basis enables a unified description of deformed and spherical nuclei, situations where the nuclei involved in the double beta decay process are both spherical, both deformed or one spherical and another deformed, can be treated through a sole formalism. Dependence of single β^- and β^+ strength distribution on atomic mass number and nuclear deformation is analyzed. For the double beta decay process, the Gamow-Teller transition amplitudes and half lives are calculated. Results are compared with the experimental data as well as with the predictions of other theoretical approaches. The agreement between the present results and experimental data is fairly good.

PACS numbers: 23.40.Hc, 23.40.-s

I. INTRODUCTION

The double beta decay of a (Z,N) nucleus, may take place through two distinct channels. For one channel, the final state consists of the residual nucleus $(Z+2,N-2)$, two electrons and two antineutrinos, while for the other one the final state is lacking the antineutrinos. Suggestively, the two decay modes are called two neutrinos double beta ($2\nu\beta\beta$) and neutrinoless ($0\nu\beta\beta$) double beta decay, respectively. The second mode is especially interesting since its discovery may provide a definite answer to the question whether neutrino is a Dirac or Majorana particle. The $2\nu\beta\beta$ process is interesting by its own but also due to the fact that may provide realistic nuclear matrix elements which might be further used to quantitatively evaluate the rate of the neutrinoless double beta decay.

For such reasons many theoreticians focused their efforts in describing consistently the data for $2\nu\beta\beta$ decay. The contributions over several decades have been reviewed by many authors. Instead of enumerating the main steps achieved toward improving the theoretical description we advise the reader to consult a few of the review works [1, 2, 3, 4, 5, 6, 7, 8].

It is interesting to note that, most of the double beta emitters are deformed nuclei, the proposed formalisms use a single particle spherical basis. More than 10 years ago, one of us [9] proposed a formalism to describe the process of two neutrinos double beta decay in a projected spherical basis. It was for the first time that a proton-neutron quasiparticle random phase approximation (pnQRPA) for a two body interaction in the ph and pp channels with a deformed single particle basis was performed. Moreover, effects which are beyond pnQRPA, have been accounted for by means of a boson expansion procedure. Few years later the influence of nuclear deformation upon the contribution of the spin-flip configurations to the Gamow-Teller double beta transition amplitude, was studied [10]. In the meantime several papers have been devoted to the extension of the pnQRPA procedure to deformed nuclei, the applications being performed for studying the single beta decay properties as well as the double beta decay rates. Thus, pnQRPA approaches using as deformed single particle basis Nilsson or deformed Woods Saxon states have been formulated[11, 12, 13, 14]. Also, a self-consistent deformed method was formulated where the single particle basis was obtained as eigenstates of a deformed mean field defined through a Hartree-Fock treatment of a density dependent two body interaction of Skyrme type [12].

In a recent publication [15] we continued the project opened in Ref.[9], by improving the

single particle basis. Indeed, in Ref.[9] the single particle energies were depending linearly on a parameter which simulates the nuclear deformation. By contrast, in Ref. [15] the core volume conservation constraint, ignored in the previous paper, determines a nonlinear deformation dependence for single particle energies. Of course, having different single particle energies, the pairing properties and the double beta matrix elements are expected to be modified. Another issue addressed in the previous paper was whether considering different deformations for the mother and daughter nuclei, modifies significantly the double beta transition amplitude (M_{GT}). The answer to this question is positive since modifying the deformation for the daughter nucleus, the ground state correlations are modified and consequently the pnQRPA collapse point is changed. On the other hand the overlap matrix elements of the states describing the intermediate odd-odd nucleus, defined as excited states from the mother and daughter ground states respectively, are decreased. Therefore, considering different nuclear deformations for mother and daughter nuclei quenches the Gamow-Teller (GT) double beta decay amplitude, which results in improving the agreement with the experimental data.

The angular momentum projected spherical basis enables a unified description of spherical and deformed nuclei. Here we use this virtue of the single particle basis defined in Ref.[15] and try to depict the specific features of the transitions between nuclei of similar or different nuclear shapes: a) spherical \rightarrow spherical ($^{48}\text{Ca} \rightarrow ^{48}\text{Ti}$), b) spherical \rightarrow deformed-prolate ($^{128}\text{Te} \rightarrow ^{128}\text{Xe}$, $^{130}\text{Te} \rightarrow ^{130}\text{Xe}$), c) spherical \rightarrow deformed- oblate ($^{134}\text{Xe} \rightarrow ^{134}\text{Ba}$, $^{136}\text{Xe} \rightarrow ^{136}\text{Ba}$), d) deformed \rightarrow spherical ($^{110}\text{Pd} \rightarrow ^{110}\text{Cd}$), e) deformed-prolate \rightarrow deformed-prolate ($^{96}\text{Zr} \rightarrow ^{96}\text{Mo}$), f) deformed-oblate \rightarrow deformed-oblate ($^{100}\text{Mo} \rightarrow ^{100}\text{Ru}$, $^{104}\text{Ru} \rightarrow ^{104}\text{Pd}$, $^{116}\text{Cd} \rightarrow ^{116}\text{Sn}$). It is worth mentioning that except for ^{104}Ru , ^{110}Pd and ^{134}Xe for all other cases experimental data are available.

The results of the present paper will be described according to the following plan. For the sake of a self-sustaining presentation, a brief review of the projected spherical single particle basis will be presented in Section II. Also, the basic equations necessary for calculating the GT double beta transition amplitude are given. In Section III, we discuss the results for ten double beta emitters: ^{48}Ca , ^{96}Zr , ^{100}Mo , ^{104}Ru , ^{110}Pd , ^{116}Cd , ^{128}Te , ^{130}Te , ^{134}Xe , ^{136}Xe , for which the strength distribution for single β^- emission, the M_{GT} and half lives values for the double beta decay process, are presented. Also, the strength distribution for the β^+ decay of the corresponding daughter nuclei is presented as function of the pnQRPA energy. A short

summary and concluding remarks are given in Section IV.

II. PNQRPA TREATMENT OF THE GT $\beta\beta$ TRANSITION AMPLITUDE

A. Projected single particle basis

In Ref. [16], one of us, (A.A.R.), introduced an angular momentum projected single particle basis which seems to be appropriate for the description of the single particle motion in a deformed mean field generated by the particle-core interaction. This single particle basis has been used to study the collective M1 states in deformed nuclei [17] as well as the rate of double beta process [9, 10]. Recently, a new version has been proposed where the deformation dependence of single particle energies is nonlinear and therefore more realistic [18, 19]. The new single particle basis has been used to study the double beta decay of deformed nuclei [15]. In order to fix the necessary notations and moreover for the sake of a self-contained presentation, we describe briefly the main ideas underlying the construction of the projected single particle basis.

The single particle mean field is determined by a particle-core Hamiltonian:

$$\tilde{H} = H_{sm} + H_{core} - M\omega_0^2 r^2 \sum_{\lambda=0,2} \sum_{-\lambda \leq \mu \leq \lambda} \alpha_{\lambda\mu}^* Y_{\lambda\mu}. \quad (2.1)$$

where H_{sm} denotes the spherical shell model Hamiltonian, while H_{core} is a harmonic quadrupole boson (b_μ^+) Hamiltonian, associated to a phenomenological core. The interaction of the two subsystems is accounted for by the third term of the above equation, written in terms of the shape coordinates $\alpha_{00}, \alpha_{2\mu}$. The quadrupole shape coordinates are related to the quadrupole boson operators by the canonical transformation:

$$\alpha_{2\mu} = \frac{1}{k\sqrt{2}} (b_{2\mu}^\dagger + (-)^\mu b_{2,-\mu}), \quad (2.2)$$

where k is an arbitrary C number. The monopole shape coordinate is to be determined from the volume conservation condition.

Averaging \tilde{H} on a given eigenstate of H_{sm} , denoted as usual by $|nljm\rangle$, one obtains a deformed quadrupole boson Hamiltonian whose eigenstate is an axially symmetric coherent state:

$$\Psi_g = \exp[d(b_{20}^+ - b_{20})]|0\rangle_b, \quad (2.3)$$

with $|0\rangle_b$ standing for the vacuum state of the boson operators and d a real parameter which simulates the nuclear deformation. On the other hand, averaging \tilde{H} on Ψ_g one obtains a single particle mean field operator for the single particle motion, similar to the Nilsson Hamiltonian. Concluding, by averaging on a factor state of the particle core space the rotational symmetry is broken and the mean field mentioned above may generate, by diagonalization, a deformed basis for treating the many body interacting systems. However, this standard procedure is tedious since the final many body states should be projected over angular momentum.

Our procedure defines first a spherical basis for the particle-core system, by projecting out the angular momentum from the deformed state

$$\Psi_{nlj}^{pc} = |nljm\rangle \Psi_g. \quad (2.4)$$

The upper index appearing in the l.h. side of the above equation suggests that the product function is associated to the particle-core system. The projected states are obtained, in the usual manner, by acting on these deformed states with the projection operator

$$P_{MK}^I = \frac{2I+1}{8\pi^2} \int D_{MK}^I(\Omega) \hat{R}(\Omega) d\Omega. \quad (2.5)$$

We consider the subset of projected states :

$$\Phi_{nlj}^{IM}(d) = \mathcal{N}_{nlj}^I P_{MI}^I[|nljI\rangle \Psi_g] \equiv \mathcal{N}_{nlj}^I \Psi_{nlj}^{IM}(d). \quad (2.6)$$

which are orthonormalized and form a basis for the particle-core system. The main properties of these projected spherical states are:

- a) They are orthogonal with respect to I and M quantum numbers.
- b) Although the projected states are associated to the particle-core system, they can be used as a single particle basis. Indeed, when a matrix element of a particle like operator is calculated, the integration on the core collective coordinates is performed first, which results in obtaining a final factorized expression: one factor carries the dependence on deformation and one is a spherical shell model matrix element. Thus, the role of the core component is to induce a quadrupole deformation for the matrix elements of the operators acting on particle degrees of freedom.
- c) The connection between the nuclear deformation and the parameter d entering the definition of the coherent state (2.3) can be obtained by requiring that the strength of the

particle-core quadrupole-quadrupole interaction be identical to the Nilsson deformed term of the mean field.

To the projected spherical states, one associates the 'deformed' single particle energies defined as average values of the particle-core Hamiltonian $H' = \tilde{H} - H_{core}$.

$$\epsilon_{nlj}^I = \langle \Phi_{nlj}^{IM}(d) | H' | \Phi_{nlj}^{IM}(d) \rangle. \quad (2.7)$$

Since the core contribution to this average value, does not depend on the quantum numbers of the single particle energy levels, it produces a constant shift for all energies. For this reason such a term is omitted in (2.7). However, when the ground state energy variation against deformation is studied, this term must be included.

In Ref.[15] it was shown that single particle energies, defined above, exhibit a nonlinear dependence on the deformation parameter d . Such a dependence is determined by the monopole-monopole interaction term after implementing the volume conservation constraint. Moreover, the deformation dependence of the new single particle energies is similar to that shown by the Nilsson model [20]. Therefore, the average values ϵ_{nlj}^I may be viewed as approximate expressions for the single particle energies in deformed Nilsson orbits [20]. We may account for the deviations from the exact eigenvalues by considering, at a later stage when a specific treatment of the many body system is performed, the exact matrix elements of the two body interaction.

Although the energy levels are similar to those of the Nilsson model, the quantum numbers in the two schemes are different. Indeed, here we generate from each j a multiplet of $(2j+1)$ states distinguished by the quantum number I , which plays the role of the Nilsson quantum number Ω and runs from $1/2$ to j . Moreover, the energies corresponding to the quantum numbers K and $-K$ are equal to each other. On the other hand, for a given I there are $2I+1$ degenerate sub-states while the Nilsson states are only double degenerate. As explained in Ref.[16], the redundancy problem can be solved by changing the normalization of the model functions:

$$\langle \Phi_{\alpha}^{IM} | \Phi_{\alpha}^{IM} \rangle = 1 \implies \sum_M \langle \Phi_{\alpha}^{IM} | \Phi_{\alpha}^{IM} \rangle = 2. \quad (2.8)$$

Due to this weighting factor the particle density function is providing the consistency result that the number of particles which can be distributed on the $(2I+1)$ sub-states is at most 2, which agrees with the Nilsson model. Here α stands for the set of shell model quantum

numbers nlj . Due to this normalization, the states Φ_α^{IM} used to calculate the matrix elements of a given operator should be multiplied with the weighting factor $\sqrt{2/(2I+1)}$.

Concluding, the projected single particle basis is defined by Eq. (2.6). Although these states are associated to a particle-core system, they can be used as a single particle basis due to the properties mentioned above. The projected states might be thought of as eigenstates of an effective rotational invariant fermionic one-body Hamiltonian H_{eff} , with the corresponding energies given by Eq.(2.7).

$$H_{eff}\Phi_\alpha^{IM} = \epsilon_\alpha^I(d)\Phi_\alpha^{IM}. \quad (2.9)$$

This definition should be supplemented by the request that the matrix elements of any operator between states Φ_α^{IM} and $\Phi_{\alpha'}^{I'M'}$ have, as we mentioned above, a factorized form, one factor carrying the d dependence, while the second one being a spherical shell model matrix element. Due to these features, these states can be used as single particle basis to treat many body Hamiltonians which involve one-body operators. This is the case of Hamiltonians with two body separable forces. As a matter of fact, such a type of Hamiltonian is used in the present paper.

As shown in Ref. [15] in the vibrational limit, $d \rightarrow 0$, the projected spherical basis goes to the spherical shell model basis and ϵ_{nlj}^I to the eigenvalues of H_{sm} .

A fundamental result obtained in Ref.[19] for the product of two single particle states, which comprises a product of two core components, deserves to be mentioned. Therein we have proved that the matrix elements of a two body interaction corresponding to the present scheme are very close to the matrix elements corresponding to spherical states projected from a deformed product state with one factor as a product of two spherical single particle states, and a second factor consisting of a common collective core wave function. The small discrepancies of the two types of matrix elements could be washed out by using slightly different strengths for the two body interaction in the two methods. Due to this property the basis (2.6) might be used for studying any two-body interaction.

B. The model Hamiltonian and its pnQRPA approach

In the present work we aim at describing the Gamow-Teller two neutrino double beta decay processes with the property that mother and daughter nuclei may exhibit different

shapes. Indeed, in the chosen cases they might be both spherical, both deformed but with different deformations or one spherical and the other one of a deformed shape. The specific feature of the formalism used in the present work consists in treating all cases in an unified manner by using a sole single particle basis.

The main ingredients of our formalism are as follows. The Fermi transitions contributing about 20% and the “forbidden” transitions are ignored, which is a reasonable approximation for the two neutrino double beta decay in medium and heavy nuclei. As usual, the $2\nu\beta\beta$ process is conceived as two successive single β^- transitions. The first transition connects the ground state of the mother nucleus to a magnetic dipole state 1^+ of the intermediate odd-odd nucleus which subsequently decays to the ground state of the daughter nucleus. The states mentioned above, involved in the $2\nu\beta\beta$ process, are described in the framework of the pnQRPA formalism, by using the following many body Hamiltonian:

$$H = \sum \frac{2}{2I+1} (\epsilon_{\tau\alpha I} - \lambda_{\tau\alpha}) c_{\tau\alpha IM}^\dagger c_{\tau\alpha IM} - \sum \frac{G_\tau}{4} P_{\tau\alpha I}^\dagger P_{\tau\alpha I} + 2\chi \sum \beta_\mu^-(pn) \beta_{-\mu}^+(p'n') (-)^\mu - 2\chi_1 \sum P_{1\mu}^-(pn) P_{-\mu}^+(p'n') (-)^\mu. \quad (2.10)$$

The operator $c_{\tau\alpha IM}^\dagger (c_{\tau\alpha IM})$ creates (annihilates) a particle of type τ ($=p,n$) in the state Φ_α^{IM} , when acting on the vacuum state $|0\rangle$. In order to simplify the notations, hereafter the set of quantum numbers $\alpha(=nlj)$ will be omitted. The two body interaction consists of three terms, the pairing, the dipole-dipole particle-hole (ph) and the particle-particle (pp) interactions. The corresponding strengths are denoted by G_τ ($\tau = p, n$), χ, χ_1 , respectively. All of them are separable interactions, with the factors defined by the following expressions:

$$\begin{aligned} P_{\tau I}^\dagger &= \sum_M \frac{2}{2I+1} c_{\tau IM}^\dagger c_{\tau IM}^\dagger, \\ \beta_\mu^-(pn) &= \sum_{M, M'} \frac{\sqrt{2}}{\hat{I}} \langle pIM | \sigma_\mu | nI'M' \rangle \frac{\sqrt{2}}{\hat{I}'} c_{pIM}^\dagger c_{nI'M'}, \\ P_{1\mu}^-(pn) &= \sum_{M, M'} \frac{\sqrt{2}}{\hat{I}} \langle pIM | \sigma_\mu | nI'M' \rangle \frac{\sqrt{2}}{\hat{I}'} c_{pIM}^\dagger c_{nI'M'}^\dagger. \end{aligned} \quad (2.11)$$

The remaining operators from Eq.(2.10) can be obtained from the above defined operators, by hermitian conjugation.

The one body term and the pairing interaction terms are treated first through the standard BCS formalism and consequently replaced by the quasiparticle one body term

$\sum_{\tau IM} E_{\tau} a_{\tau IM}^{\dagger} a_{\tau IM}$. In terms of quasiparticle creation ($a_{\tau IM}^{\dagger}$) and annihilation ($a_{\tau IM}$) operators, related to the particle operators by means of the Bogoliubov-Valatin transformation, the two body interaction terms, involved in the model Hamiltonian, can be expressed just by replacing the operators (2.11) by their quasiparticle images which at their turn can be expressed as linear combination of dipole two quasiparticle and quasiparticle density operators defined as:

$$\begin{aligned} A_{1\mu}^{\dagger}(pn) &= \sum_{m_p, m_n} C_{m_p m_n}^{I_p I_n 1} a_{p I_p m_p}^{\dagger} a_{n I_n m_n}^{\dagger}, \\ B_{1\mu}^{\dagger}(pn) &= \sum_{m_p, m_n} C_{m_p -m_n}^{I_p I_n 1} a_{p I_p m_p}^{\dagger} a_{n I_n m_n} (-)^{I_n - m_n} = -[a_{p I_p}^{\dagger} a_{n I_n}^{\dagger}]_{1\mu}. \end{aligned} \quad (2.12)$$

The quasiparticle Hamiltonian is further treated within the pnQRPA formalism, i.e. one determines the operator

$$\Gamma_{1\mu}^{\dagger} = \sum_k [X(k) A_{1\mu}^{\dagger}(k) - Y(k) A_{1,-\mu}(k) (-)^{1-\mu}], \quad (2.13)$$

which satisfies the restrictions:

$$[\Gamma_{1\mu}, \Gamma_{1\mu'}^{\dagger}] = \delta_{\mu, \mu'}, \quad [H_{qp}, \Gamma_{1\mu}^{\dagger}] = \omega \Gamma_{1\mu}^{\dagger}. \quad (2.14)$$

These operator equations yield a set of algebraic equations for the X (usually called forward going) and Y (named back-going) amplitudes:

$$\begin{pmatrix} \mathcal{A} & \mathcal{B} \\ -\mathcal{B} & -\mathcal{A} \end{pmatrix} \begin{pmatrix} X \\ Y \end{pmatrix} = \omega \begin{pmatrix} X \\ Y \end{pmatrix}, \quad (2.15)$$

$$\sum_k [|X(k)|^2 - |Y(k)|^2] = 1. \quad (2.16)$$

The analytical expressions for the pnQRPA matrices \mathcal{A} and \mathcal{B} are given in Ref.[15]. Since the pp interaction has an attractive character, for a critical value of χ_1 the lowest root of the pnQRPA equations may become imaginary. Suppose that χ_1 is smaller than its critical value and therefore all RPA solutions (i.e. ω) are real numbers and ordered as:

$$\omega_1 \leq \omega_2 \leq \dots \leq \omega_{N_s}. \quad (2.17)$$

Here N_s stands for the total number of the proton-neutron pair states whose angular momenta can couple to 1^+ and moreover their quantum numbers n, l are the same. Hereafter

the phonon amplitudes X and Y will be accompanied by a lower index “ i ” suggesting that they correspond to the energy ω_i .

Since our single particle basis states depend on the deformation parameter d , so do the pnQRPA energies and amplitudes. The pnQRPA ground state (the vacuum state of the pnQRPA phonon operator) describes an even-even system which might be either the mother or the daughter nucleus. In the two cases the gauge and nuclear deformation properties are different which results in determining distinct pnQRPA phonon operators acting on different vacua describing the mother and daughter ground states, respectively. Therefore, one needs an additional index distinguishing the phonon operators of the mother and daughter nuclei. The single phonon states are defined by the equations:

$$|1_k\mu\rangle_j = \Gamma_{jk;1\mu}^\dagger |0\rangle_j, \quad j = i, f; \quad k = 1, 2, \dots, N_s. \quad (2.18)$$

Here the indices i and f stand for initial (mother) and final (daughter) nuclei, respectively. This equation defines two sets of non-orthogonal states, $\{|1_k\mu\rangle_i\}$ and $\{|1_k\mu\rangle_f\}$ describing the neighboring odd-odd nucleus. The states of the first set may be fed by a beta minus decay of the ground state of the mother nucleus while the states of the second set are populated with a beta plus transition operator from the ground state of the daughter nucleus.

If the energy carried by leptons in the intermediate state is approximated by the sum of the rest energy of the emitted electron and half the Q-value of the double beta decay process

$$\Delta E = \frac{1}{2}Q_{\beta\beta} + m_e c^2, \quad (2.19)$$

the reciprocal value of the $2\nu\beta\beta$ half life can be factorized as:

$$(T_{1/2}^{2\nu\beta\beta})^{-1} = F |M_{GT}(0_i^+ \rightarrow 0_f^+)|^2, \quad (2.20)$$

where F is an integral on the phase space, independent of the nuclear structure, while M_{GT} stands for the Gamow-Teller transition amplitude and has the expression :

$$M_{GT} = \sqrt{3} \sum_{kk'} \frac{i \langle 0 | \beta_i^+ | 1_k \rangle_{ii} \langle 1_k | 1_{k'} \rangle_{ff} \langle 1_{k'} | \beta_f^+ | 0 \rangle_f}{E_k + \Delta E + E_{1+}}. \quad (2.21)$$

In the above equation, the denominator consists of three terms: a) ΔE , which was already defined, b) the average value of the k -th pnQRPA energy normalized to the particular value corresponding to $k=1$, i.e.

$$E_k = \frac{1}{2}(\omega_{i,k} + \omega_{f,k}) - \frac{1}{2}(\omega_{i,1} + \omega_{f,1}), \quad (2.22)$$

and c) the experimental energy for the lowest 1^+ state. The indices carried by the transition operators indicate that they act in the space spanned by the pnQRPA states associated to the initial (i) or final (f) nucleus. The overlap matrix elements of the single phonon states in the mother and daughter nuclei respectively, are calculated within the pnQRPA approach and have the expressions:

$${}_i\langle 1_k | 1_{k'} \rangle_f = \sum_{pn} [X_k(i, pn)X_{k'}(f, pn) - Y_k(i, pn)Y_{k'}(f, pn)]. \quad (2.23)$$

Throughout this paper, the Rose [22] convention for the Wigner Eckart theorem is used.

Before closing this section we would like to say a few words about what is specific to our formalism. Since our single particle states are projected spherical states, the pnQRPA formalism is fully identical to the one, usually employed for spherical nuclei. Since in the vibrational limit, ($d \rightarrow 0$), our basis goes to the spherical shell model basis, one may say that the present formalism provides a unified description of spherical and deformed nuclei.

III. NUMERICAL RESULTS

The formalism described in the previous section, has been applied to the following ten isotopes: ^{48}Ca , ^{96}Zr , ^{100}Mo , ^{104}Ru , ^{110}Pd , ^{116}Cd , ^{128}Te , ^{130}Te , ^{134}Xe , ^{136}Xe . The spherical shell model parameters for these double beta emitters and the corresponding daughter nuclei are given by:

$$\hbar\omega_0 = 41A^{1/3}, \quad C = 2\hbar\omega_0\kappa, \quad D = \hbar\omega_0\mu, \quad (3.1)$$

with the strength parameters κ and μ having the same (Z,N) dependence as in Ref. [23].

The angular momentum projected basis depends on two additional parameters. These are the deformation parameter d and the factor k entering the canonical transformation relating the quadrupole coordinate and boson operators. They are fixed in the same manner as in our previous publication [15]. Indeed, we require that the relative energy for the states $|1f_{\frac{7}{2}}^{\frac{7}{2}}\rangle$ and $|1d_{\frac{5}{2}}^{\frac{1}{2}}\rangle$ be equal to that of Nilsson levels with $\Omega = \frac{7}{2}$ and $\Omega = \frac{1}{2}$ in the $N = 3$ major shell. Moreover, adding to the mean field term defined before a QQ two body interaction we require that the lowest root for the charge conserving QRPA equation be equal to the

experimental energy of the lowest 2^+ state in the mother nucleus. Throughout this paper, the M-degenerate states Φ_{nlj}^{IM} are denoted by $|n + 1 \ ljI\rangle$.

The BCS calculation has been performed within a restricted single particle space. Due to the level crossing, the restriction of the single particle space for deformed nuclei is different from that for spherical nuclei. Indeed, in spherical nuclei Ikeda sum rule (ISR) is satisfied if two major shells plus the spin orbit partner of the intruder state are included in the single particle space. Suppose that the neutron open shell has $N=3$ with the intruder state $|1g9/2\rangle$, in the standard spherical shell model picture. In the present formalism, including the spin-orbit partner state $|1g7/2\rangle$ means to consider the states $\Phi_{0,4,\frac{7}{2}}^{IM}$ with $I = 7/2, 5/2, 3/2, 1/2$. However, some of these states are higher in energy than states belonging to the $|2d5/2I\rangle$ multiplet. Due to such features appearing both in the upper part of the major open shell of neutrons and the bottom side of the proton major open shell we truncated the space considering an inert (Z,N) core and a number of states lying above the core states. The core and the number of outside states are chosen such that the non-occupation probabilities for the neglected bottom states as well as the occupation probabilities for the ignored upper states are smaller than 0.01. Of course, the single particle space for protons and neutrons are the same. Our calculations were performed with the core and number of states given in Table I. Once the single particle space is defined, the number of the dipole proton-neutron states can be calculated. Furthermore, the dimensions of the pnQRPA matrices for mother (D_1) and daughter (D_2) nuclei are readily obtained. These dimensions are also given in Table I. It is worth mentioning that using the single particle spaces given in Table I, Ikeda sum rule is satisfied for both the mother and daughter nuclei considered in the present paper.

Nucleus	^{48}Ca	^{96}Zr	^{100}Mo	^{104}Ru	^{110}Pd	^{116}Cd	^{128}Te	^{130}Te	^{134}Xe	^{136}Xe
The (Z,N) core	(0,0)	(20,20)	(26,26)	(26,26)	(26,26)	(26,26)	(44,44)	(44,44)	(44,44)	(44,44)
Number of states	19	20	20	22	23	27	22	23	21	23
D_1	118	128	132	140	154	166	142	150	138	154
D_2	115	128	132	140	154	166	128	132	120	140

TABLE I: The number of single particle proton states lying above the (Z,N) core is given. The single particle space for neutrons is identical to that for protons. D_1 and D_2 are the dimensions of the pnQRPA matrix for mother and daughter nuclei, respectively

Note that despite the fact that single particle energies have a deformation dependence, we keep calling a major shell a set of states characterized by the same quantum number $N(= 2n + l)$ plus the states from the shell $N + 1$ of maximum j .

Single particle parameters d and k as well as the pairing strengths, fixed so that the mass difference of the neighboring even-even nuclei are reproduced, are listed in Table III.

Now, let us turn our attention to the proton-neutron dipole interactions. In Ref[11] it was suggested a simple A-dependence for these interaction strengths:

$$\chi = \frac{5.2}{A^{0.7}}MeV, \quad \chi_1 = \frac{0.58}{A^{0.7}}MeV. \quad (3.2)$$

We recall that this A dependence of the proton-neutron ph interaction strengths was obtained by fitting the position of the GT resonance for ^{40}Ca , ^{90}Zr and ^{208}Pb . The pp interaction strength given above has been obtained by fitting the half lives for $Z \leq 40$ nuclei against the single β^+ decay. A certain caution, however, is necessary when these formulae are used, since the A dependence is conditioned by the mass region [28] as well as by the single particle space [26, 27]. For example, in Ref.[51] the GT resonance centroids in ^{128}Te and ^{130}Te , located at 13.7 and 14.1 MeV respectively, are reproduced with the χ values equal to 0.157 and 0.16 MeV respectively. These values for χ are different from the predictions of Eq.(3.2) corresponding to A=128 and A=130, respectively. Moreover, as we see from Table IV, in the current paper the right position of these GT resonances are obtained by using $\chi = 0.268$ for both isotopes. It is noteworthy the fact that the daughter nuclei involved in a double beta process are stable against β^+ transitions. Therefore χ_1 is to be determined either using information about the half life of a β^+ emitter lying close, in the nuclide chart, to the daughter nucleus under consideration or by fitting the data for a (p,n) reaction having the daughter as a residual nucleus. Hereafter, the ratio χ/χ_1 is denoted, as usual, by g_{pp} .

The adopted procedure to fix the proton-neutron dipole interaction strengths is as follows. Whenever, in the intermediate odd-odd nucleus, the position of the GT resonance centroid is known, the ph interaction strength is fixed so that the above mentioned data is reproduced. As shown in Table II, for some of the isotopes considered in the present paper the $\log ft$ values associated to the β^+/EC and β^- transitions of the corresponding intermediate nuclei, are experimentally known. For these particular cases, χ and g_{pp} are fixed by fitting the two mentioned experimental data. The $\log ft$ values were calculated by using the following

Mother nucleus	Transition $\log ft$	Intermediate nucleus	Transition $\log ft$	Daughter nucleus
^{100}Mo	$\beta^+/\overleftarrow{EC}$ Exp. $4.45^{+0.18}_{-0.30}$ <i>f)</i> Th. 4.61	^{100}Tc	$\beta^-/\overrightarrow{}$ 4.66 <i>a)</i> 4.66	^{100}Ru
^{104}Ru	$\beta^+/\overleftarrow{EC}$ Exp. 4.32 <i>b)</i> Th. 4.20	^{104}Rh	$\beta^-/\overrightarrow{}$ 4.55 <i>b)</i> 4.62	^{104}Pd
^{110}Pd	$\beta^+/\overleftarrow{EC}$ Exp. 4.08 <i>c)</i> Th. 3.86	^{110}Ag	$\beta^-/\overrightarrow{}$ 4.66 <i>c)</i> 4.83	^{110}Cd
^{116}Cd	$\beta^+/\overleftarrow{EC}$ Exp. $4.39^{+0.1}_{-0.15}$ <i>g)</i> Th. 4.05	^{116}In	$\beta^-/\overrightarrow{}$ 4.662 <i>d)</i> 4.670	^{116}Sn
^{128}Te	$\beta^+/\overleftarrow{EC}$ Exp. 5.049 <i>h)</i> Th. 4.930	^{128}I	$\beta^-/\overrightarrow{}$ 6.061 <i>e)</i> 6.226	^{128}Xe

TABLE II: The experimental and theoretical $\log ft$ values characterizing the $\beta^+/\overleftarrow{EC}$ and β^- processes of the intermediate nucleus ground state (1^+). Experimental data are from: *a)*[43], *b)*[44], *c)*[45], *d)*[46], *e)*[47], *f)*[65], *g)*[66], *h)*[67]

expression for ft :

$$ft_{\mp} = \frac{6160}{[{}_l\langle 1_1 || \beta^{\pm} || 0 \rangle_l g_A]^2}. \quad (3.3)$$

Here $|1_1 M\rangle$ denotes the first dipole phonon state in the intermediate odd-odd nucleus while $|0\rangle$ is the pnQRPA ground state. The low index "l" may take the value "i" and "f" depending whether the end state of the transition is characterizing the double beta mother or daughter nucleus. Therefore $l = f$ is associated to single β^- transition, while $l = i$ to the $\beta^+/\overleftarrow{EC}$ process. We chose $g_A = 1.0$ in order to take account of the effect of distant states responsible for the "missing strength" in the giant GT resonance [1]. For ^{48}Ca , we considered first χ and g_{pp} (second row of Table IV) as given by Eq.(3.2). To see the effect

of g_{pp} on M_{GT} we repeated the calculations by keeping the same χ as before but taking $g_{pp} = 0$ (third row of Table IV). It seems that fixing χ as to reproduce the GT resonance centroid and taking $g_{pp} = 0$ yields a better agreement with the experimental data. This situation is presented in the first row of Table IV. For ^{96}Zr , χ was fixed by fitting the energy for the GT resonance centroid, while g_{pp} was taken as required by Eq.3.2. For ^{130}Te we took the same χ and g_{pp} as for ^{128}Te . It is interesting to note that for this value of χ the position of the GT resonance, at 14.1 Mev is nicely reproduced. As for the last two double beta emitters included in Table IV, there are available data neither for the GT resonance nor for the $\log ft$ values characterizing the single β^- and β^+/EC transitions of the corresponding intermediate odd-odd nuclei. For these isotopes we supposed for χ and g_{pp} a similar linear $1/A$ dependence as for ^{130}Te .

The strength parameters χ and g_{pp} determined in the manner described above are collected in Table III. They are also listed for each isotope in the first row of Table IV. These parameters yield double beta half-lives which are to be compared with the corresponding experimental data. The same parameters are used to calculate the single beta strength distributions, shown in Figs 1-4. However, in order to have a fair comparison of the present results and those of Klapdor *et al.*[36, 37, 39], in the second row of Table IV we give the results obtained with χ and χ_1 given by Eq.(3.2).

Once the parameters involved in the model Hamiltonian are fixed, the BCS and pnQRPA equations can be solved and the results be used in Eq.(2.21) to calculate the M_{GT} amplitude. Further, Eq.(2.20) is used to calculate the half life of the $2\nu\beta\beta$ process. The phase factor F is not depending on the nuclear state structure and therefore was taken as in Refs.[1, 53]. The values for F , used in this paper, correspond to $g_A = 1.254$ (see the comments at the end of this section). Results for M_{GT} and $T_{1/2}$ are given in Table IV. Therein one may find also the available experimental data.

Nucleus	d	k	G_p [MeV]	G_n [MeV]	χ [MeV]	g_{pp}	$(\frac{1}{2}Q_{\beta\beta} + m_e c^2)$ [MeV]
^{48}Ca	0.3	10.00	0.65	0.45	0.180	0.0	2.646
^{48}Ti	0.05	2.00	0.46	0.36	0.180	0.0	
^{96}Zr	1.5	10.20	0.26	0.26	0.5	0.112	2.186
^{96}Mo	1.2	7.20	0.3	0.3	0.5	0.112	
^{100}Mo	-1.4	10.00	0.28	0.26	0.060	1.600	2.026
^{100}Ru	-0.6	3.6	0.285	0.220	0.060	1.600	
^{104}Ru	-1.55	8.80	0.26	0.2	0.150	2.750	1.161
^{104}Pd	-1.35	6.94	0.26	0.180	0.150	2.750	
^{110}Pd	-1.6	6.00	0.30	0.32	0.148	2.450	1.516
^{110}Cd	-0.8	3.06	0.30	0.18	0.148	2.450	
^{116}Cd	-1.8	3.00	0.20	0.245	0.238	1.680	1.916
^{116}Sn	-1.2	2.50	0.18	0.275	0.238	1.680	
^{128}Te	0.5	1.62	0.27	0.220	0.268	1.250	0.946
^{128}Xe	1.7	6.50	0.23	0.220	0.268	1.250	
^{130}Te	0.493	1.88	0.24	0.210	0.268	1.300	1.776
^{130}Xe	1.4	5.00	0.24	0.205	0.268	1.300	
^{134}Xe	-0.1	1.95	0.28	0.300	0.260	1.261	0.931
^{134}Ba	-0.468	1.50	0.24	0.240	0.260	1.261	
^{136}Xe	-0.1	1.80	0.23	0.29	0.256	1.243	1.751
^{136}Ba	-0.698	2.16	0.19	0.20	0.256	1.243	

TABLE III: The pairing and Gamow Teller ph interaction strengths are given in units of MeV. The ratio of the two dipole interaction (particle-hole and particle-particle) strengths, denoted by g_{pp} , is also given. The list of the deformation parameter d and the factor k of the transformation (2.2) are also presented. The manner in which these parameters were fixed is explained in the text.

$2\nu\beta\beta$ decay	χ [MeV]	g_{pp}	$ M_{GT} $ [MeV $^{-1}$]	$T_{1/2}$ [yr]			
				present	exp.	Suhonen et al.	Klapdor et al.
$^{48}\text{Ca} \rightarrow ^{48}\text{Ti}$	0.180	0.0	0.043	$5.23 \cdot 10^{19}$	$(4.2 \pm 1.2) \cdot 10^{19}$ a)		$3.2 \cdot 10^{19}$ 1)
	0.346	0.112	0.032	$9.27 \cdot 10^{19}$			
	0.346	0.0	0.036	$7.48 \cdot 10^{19}$			
$^{96}\text{Zr} \rightarrow ^{96}\text{Mo}$	0.500	0.112	0.113	$1.66 \cdot 10^{19}$	$(1.4_{-0.5}^{+3.5}) \cdot 10^{19}$ a)	$0.44 \cdot 10^{20}$ 2)	$5.2 \cdot 10^{17}$
	0.213	0.112	0.219	$0.44 \cdot 10^{19}$			
$^{100}\text{Mo} \rightarrow ^{100}\text{Ru}$	0.060	1.600	0.305	$4.61 \cdot 10^{18}$	$(8.0 \pm 0.6) \cdot 10^{18}$ a)	$2.9 \cdot 10^{18}$ 3)	$1.8 \cdot 10^{18}$
	0.207	0.112	0.212	$9.55 \cdot 10^{18}$	$(0.115_{-0.02}^{+0.03}) \cdot 10^{20}$ b)		
					$(0.033_{-0.01}^{+0.02}) \cdot 10^{20}$ c,d)		
$^{104}\text{Ru} \rightarrow ^{104}\text{Pd}$	0.150	2.750	0.781	$0.76 \cdot 10^{21}$			$1.8 \cdot 10^{21}$
	0.201	0.112	0.343	$3.95 \cdot 10^{21}$			$3.09 \cdot 10^{22}$ 6)
$^{110}\text{Pd} \rightarrow ^{110}\text{Cd}$	0.148	2.45	0.263	$15.85 \cdot 10^{19}$			$5.0 \cdot 10^{19}$
	0.194	0.112	0.218	$22.99 \cdot 10^{19}$			$1.24 \cdot 10^{21}$ 6)
$^{116}\text{Cd} \rightarrow ^{116}\text{Sn}$	0.238	1.680	0.116	$3.86 \cdot 10^{19}$	$(3.2 \pm 0.3) \cdot 10^{19}$ a)	$5.1 \cdot 10^{19}$ 5)	$8.3 \cdot 10^{18}$
	0.187	0.112	0.069	$10.96 \cdot 10^{19}$			$3.75 \cdot 10^{19}$ 4)
$^{128}\text{Te} \rightarrow ^{128}\text{Xe}$	0.268	1.250	0.090	$0.55 \cdot 10^{24}$	$(7.2 \pm 0.3) \cdot 10^{24}$ a)	$5.6 \cdot 10^{23}$ 5)	$1.2 \cdot 10^{23}$
	0.174	0.112	0.127	$0.28 \cdot 10^{24}$	$(1.5 \pm 0.2) \cdot 10^{24}$ e)		$5.7 \cdot 10^{23}$ *)
$^{130}\text{Te} \rightarrow ^{130}\text{Xe}$	0.268	1.300	0.055	$0.261 \cdot 10^{21}$	$(1.5 - 2.8) \cdot 10^{21}$ b)	$0.26 \cdot 10^{21}$ 5)	$1.9 \cdot 10^{19}$
	0.172	0.112	0.091	$0.097 \cdot 10^{21}$	$(2.7 \pm 0.1) \cdot 10^{21}$ a)		$1.2 \cdot 10^{20}$ *)
					$(0.75 \pm 0.3) \cdot 10^{21}$ f)		
$^{134}\text{Xe} \rightarrow ^{134}\text{Ba}$	0.260	1.261	0.039	$3.75 \cdot 10^{24}$			$5.1 \cdot 10^{22}$
	0.169	0.112	0.040	$3.49 \cdot 10^{24}$			$2.5 \cdot 10^{23}$ *)
$^{136}\text{Xe} \rightarrow ^{136}\text{Ba}$	0.256	1.243	0.039	$5.102 \cdot 10^{20}$	$> 8.1 \cdot 10^{20}$ a)	$1.3 \cdot 10^{20}$ 5)	$6.0 \cdot 10^{19}$
	0.167	0.112	0.068	$1.69 \cdot 10^{20}$			$3.3 \cdot 10^{19}$ *)

TABLE IV: The Gamow-Teller amplitude for the $2\nu\beta\beta$ decay, in units of MeV $^{-1}$, and the corresponding half life ($T_{1/2}$), in units of *yr*, are listed for ten ground to ground transitions. The experimental half lives for the transitions of ^{48}Ca (^aRef.[24]), ^{96}Zr (^a Ref. [24]), ^{100}Mo (^a Ref.[24], ^b Ref.[29] ^c Ref.[30], ^c Ref.[31]), ^{116}Cd (^a Ref.[24]), ^{128}Te (^a Ref.[24], ^e Ref.[32]), ^{130}Te (^a Refs.[24], ^b Refs.[29], ^f Ref.[33]), ^{136}Xe (^a Refs.[24]) are also given. In the second last column the results reported in Refs.[1] ²⁾, [34] ³⁾ and [35] ⁵⁾ are given. Comparison is also possible with the theoretical results from the last column reported in Refs.[36] (unmarked),[39] (¹), [37] (⁶), and [38, 58] (*). The parameters χ and a_{ex} are also given.

Before discussing the results presented in Table IV, we would like to discuss the strength distribution for single β^- and β^+ transitions of mother and daughter nuclei, respectively. Thus, in Figs. 1-4 the strengths $B'(GT)_-$ and $B'(GT)_+$ for mother and daughter nuclei respectively, folded with a gaussian having the width equal to 1 MeV, are plotted as function of pnQRPA energies. These are equal to one third of the β^- and β^+ strengths respectively, in the standard definition. Thus, the difference between the total strengths $B'(GT)_-$ and $B'(GT)_+$, characterizing the mother nucleus, is to be compared with the sum rule (N-Z). The results of our calculations are to be compared with the available data for the GT giant resonance and single beta strengths given in Refs.[51, 52, 54]. At a glance one may see that while for Te and Xe isotopes most of the strength is concentrated in a narrow resonance, for the remaining nuclei the GT resonances have a complex structure being spread over a large energy interval. Actually this feature is in agreement with experimental data showing in ^{128}I and ^{130}I a single peak at 13.7 and 14.1 MeV respectively [51] while in ^{100}Tc and ^{116}In [52] two peaks at (7.8,13.2) and (8.8, 14.30) MeV. The location of the above mentioned peaks are reasonable well reproduced. In the case of ^{100}Mo , the first peak is higher than that centered at 12.3 MeV. Increasing the value of the repulsive ph interaction χ , the ordering of the two peaks magnitudes is changed.

The β^- and β^+ strengths of ^{48}Ca have been studied in Refs.[54] and [52]. Thus, the GT resonance has been populated in the reaction $^{48}\text{Ca}(p,n)^{48}\text{Sc}$. This resonance is spread over an energy interval between 4.5 and 14.5 MeV. The result presented for $B'(GT)_-$ in Fig.1 upper left panel, agrees with the experimental data. The total β^- strength quenched with a factor of 0.6 [55], accounting for the polarization effects on the single beta transition operator, ignored in the present paper, is compared with the corresponding data in Table V. As shown therein, the agreement between the calculated strength and the corresponding data is reasonably good. The only known data for the total β^+ GT strength is for ^{48}Ti :

$$\sum B(GT)_+ = 1.42 \pm 0.2 \quad (3.4)$$

Our calculations, corresponding to the first row of Table IV, predict for this strength the value 2.59.

Comparing the β^- strength distribution among 2qp states with those corresponding to pnQRPA states, one may conclude that the quasiparticle correlations accounted for by the pnQRPA approach, favors the displacement of the strength toward higher energies. This,

in fact, is due to the repulsive character of the ph interaction. As shown in Figs. 1-4, this effect is more pronounced for ^{96}Zr , $^{128,130}\text{Te}$ and $^{134,136}\text{Xe}$.

From Table VI, it results that most of the β^- strength is due to the transitions relating the proton and neutron g states. By contrast in ^{48}Ca , ^{96}Zr and ^{116}Cd the single particle decays involving f states carry most of the transition strength. Also the GT resonance peak in ^{130}Te is determined mainly by the transition in the 2d state. While in the lighter isotopes the transitions $\nu I \rightarrow \pi I'$ where either I and I' are equal to $\frac{1}{2}$ or $\frac{3}{2}$ prevail, in Te and Xe isotopes the transitions $\nu \frac{7}{2} \rightarrow \pi \frac{5}{2}$ and $\nu \frac{5}{2} \rightarrow \pi \frac{7}{2}$ are dominant.

Concerning the β^+ strength distribution shown in Figs. 1-4, right panels, the following features are to be noticed. The magnitude of this strength is much smaller than that of β^- shown in the left panels. Moreover, the final states in the β^+ process are lying in the lower part of the spectrum, below 7.5 MeV. This suggests that the pp interaction may strongly influence the strength distribution among these states. The sensitivity of β^+ decay rate against the pp interaction was first noticed in Ref.[56]. Due to this feature the $\beta\beta$ transition amplitude is also significantly affected by increasing g_{pp} . Since the ph and pp interactions are of different nature, one is repulsive and the other one attractive, one expects that the two interactions have opposite effects on the β^+ strength. When the pp interaction is large, comparing it with the ph interaction, the β^+ strength in the quasiparticle picture is shifted toward the lower states. These are the cases of ^{104}Pd , ^{110}Cd , ^{116}Sn . When both the ph and pp interactions are large, the β^+ strength of 2qp states are very much suppressed in the pnQRPA approach. Such situations are met for $^{128,130}\text{Xe}$, and $^{134,136}\text{Ba}$.

By inspecting Table VIII, we conclude that the largest β^+ strength is carried by the single particle proton-neutron transition in the shells 1g (for ^{100}Ru , ^{104}Pd , ^{116}Sn , ^{128}Xe , ^{136}Ba), 2d (for ^{96}Mo , ^{110}Cd), 1f (for ^{48}Ti), 2f (for ^{134}Ba) and 1h (in ^{130}Xe). Identifying the common 2qp configurations carrying most efficiently the β^- and β^+ strengths from Table VI and VIII respectively, one may conclude which pnQRPA states excited from the mother and daughter ground state respectively, do maximally overlap each other and therefore bring large contribution to the double beta decay. In some of the depicted cases the state excited by the β^- transition operator belongs to the GT resonance. An excellent example on this line is that of the transition $^{48}\text{Ca} \rightarrow ^{48}\text{Ti}$, where the state at 10.326 excited from the ground state of ^{48}Ca , and that with energy of 5.957, excited from ^{48}Ti , have maximal overlap due to the 2qp state $\pi(3p\frac{1}{2}\frac{1}{2}), \nu(3p\frac{3}{2}\frac{3}{2})$ which, in both β^- and β^+ transitions, carries a large

strength.

Let us now focus our attention on the GT double beta transition amplitude. This was calculated by means of Eq.(2.21), where the energy shifts (2.19) are those listed in Table III and the measured values for 1^+ are collected in Table X. The states, energies and overlap matrix elements involved in the M_{GT} expression, were calculated within the pnQRPA approach. The results corresponding to various sets of proton-neutron dipole interactions, fixed in the manner explained before, are listed in Table IV. Therein, the half lives of the $2\nu\beta\beta$ process are also given. The agreement with the available data is fairly good.

Comparing our results with those of Klapdor *et al.*[36, 37, 58] one may say that the half lives predicted by the present paper with the dipole interaction strengths given by Eq.(3.2) are, without any exception, larger by a factor ranging from 2 (^{100}Mo) to 31 (^{96}Zr). Note that projecting out the gauge symmetry the results for Te isotopes are close to those given here for low values of g_{pp} . Comparing the results corresponding to χ and g_{pp} fixed by fitting either the GT resonance centroid energy or the $\log ft$ value for β^+ / EC transition of the odd-odd nucleus, and the $\log ft$ value of the β^- decay ending with the $\beta\beta$ daughter nucleus, with those obtained with a renormalised pnQRPA equations and an adjusted Woods Saxon single particle mean field, we note that they are close to each other.

Note that for ^{48}Ca the sets of (χ, g_{pp}) , listed in the last two rows, provide half lives larger than experimental data, which suggests that the value of χ must be smaller than required by Eq. (3.2). Indeed, decreasing χ to the value given in the first row of Table IV ($=1.80$), the agreement between the calculated GT resonance energy and the measured GT centroids could be improved. Moreover, the agreement with experimental data concerning $T_{1/2}$ is also improved. By comparison one can see that the agreement quality obtained in the present paper is similar to that yielded by a full shell model calculation in Ref.[39]. For this set of dipole interaction strengths, the quenched total strengths of β^- transition of ^{48}Ca and β^+ transition of ^{48}Ti are equal to 15.65 and 2.59 respectively. The dominant peaks in the β^- distribution correspond to the pnQRPA energies of 6.63 and 12.61 MeV. The carried strengths are 1.154 and 3.344 respectively.

An interesting feature for the decay of ^{48}Ca was pointed out by the shell model studies [39, 62, 63]. This refers to the cumulative effect brought by the low lying states in ^{48}Sc , which actually yield the bulk contribution to the matrix element. The higher 1^+ states have a coherent destructive effect on the matrix element. It is worth investigating these aspects

within the present formalism. Indeed, in Fig.5 we plotted the transition amplitude M_{GT} as a function of the upper limit of energies included in the defining equation (2.21). In other words, for a given E the energy E_k defined by Eq. (2.22) and involved in the M_{GT} expression, is restricted by $E_k \leq E$. We note that in five energy intervals this function is a monotonically increasing function of E , while in the following interval the transition amplitude decreases when states of higher energy are added. Also one notices a saturation effect, namely the contribution of states with energy larger than 16 MeV is very small. One may conclude that our results concerning the behavior of the double beta transition amplitude, are on a par with those of the shell model calculations. It is remarkable the fact that the maxima of $M_{GT}(E)$ and β^- strength are reached for similar energies.

Nucleus	⁴⁸ Ca	⁹⁶ Zr	¹⁰⁰ Mo	¹⁰⁴ Ru	¹¹⁰ Pd	¹¹⁶ Cd	¹²⁸ Te	¹³⁰ Te	¹³⁴ Xe	¹³⁶ Xe
$0.6 \sum B(GT)_-$	15.650	28.886	30.040	29.527	33.172	38.051	43.340	47.059	47.028	50.703
$\sum B(GT)_-^{exp}$	-	-	26.690	-	-	32.700	40.080	45.900	-	-

TABLE V: Total strengths for the Gamow-Teller β^- transition (first row) are compared with the available experimental data (second row). Theoretical results are quenched with a factor of 0.6. Data for ¹⁰⁰Mo and ¹¹⁶Cd are from Ref.[52] while those for ^{128,130}Te are from Ref.[51].

Nucleus	1st peak		2nd peak		3rd peak	
	Transition	Strength	Transition	Strength	Transition	Strength
⁴⁸ Ca	$\nu(3f\frac{7}{2}\frac{5}{2}) \rightarrow \pi(3f\frac{7}{2}\frac{7}{2})$	1.155	$\nu(3p\frac{3}{2}\frac{3}{2}) \rightarrow \pi(3p\frac{3}{2}\frac{1}{2})$	0.519	$\nu(3p\frac{3}{2}\frac{3}{2}) \rightarrow \pi(3p\frac{1}{2}\frac{1}{2})$	0.700
					$\nu(3f\frac{5}{2}\frac{3}{2}) \rightarrow \pi(3f\frac{7}{2}\frac{1}{2})$	3.344
⁹⁶ Zr	$\nu(3f\frac{5}{2}\frac{5}{2}) \rightarrow \pi(3f\frac{5}{2}\frac{3}{2})$	0.602	$\nu(3f\frac{7}{2}\frac{7}{2}) \rightarrow \pi(3p\frac{5}{2}\frac{5}{2})$	1.040	$\nu(3f\frac{5}{2}\frac{5}{2}) \rightarrow \pi(3f\frac{7}{2}\frac{3}{2})$	5.842
	$\nu(4d\frac{5}{2}\frac{3}{2}) \rightarrow \pi(4d\frac{5}{2}\frac{5}{2})$	0.467	$\nu(3f\frac{5}{2}\frac{5}{2}) \rightarrow \pi(3f\frac{7}{2}\frac{5}{2})$	2.473	$\nu(3f\frac{7}{2}\frac{5}{2}) \rightarrow \pi(3f\frac{5}{2}\frac{3}{2})$	2.212
			$\nu(3p\frac{1}{2}\frac{1}{2}) \rightarrow \pi(3p\frac{3}{2}\frac{3}{2})$	0.786		
¹⁰⁰ Mo	$\nu(4g\frac{9}{2}\frac{7}{2}) \rightarrow \pi(4g\frac{9}{2}\frac{9}{2})$	4.950	$\nu(4d\frac{5}{2}\frac{5}{2}) \rightarrow \pi(4d\frac{3}{2}\frac{3}{2})$	1.456	$\nu(4g\frac{9}{2}\frac{9}{2}) \rightarrow \pi(4g\frac{7}{2}\frac{7}{2})$	0.702
	$\nu(4g\frac{7}{2}\frac{7}{2}) \rightarrow \pi(4g\frac{9}{2}\frac{9}{2})$	0.428			$\nu(3f\frac{7}{2}\frac{3}{2}) \rightarrow \pi(3f\frac{5}{2}\frac{1}{2})$	0.716
	$\nu(4d\frac{5}{2}\frac{3}{2}) \rightarrow \pi(4d\frac{5}{2}\frac{1}{2})$	1.005				
¹⁰⁴ Ru	$\nu(4d\frac{3}{2}\frac{3}{2}) \rightarrow \pi(4d\frac{5}{2}\frac{1}{2})$	1.342	$\nu(4g\frac{9}{2}\frac{3}{2}) \rightarrow \pi(4g\frac{7}{2}\frac{5}{2})$	0.885	$\nu(4g\frac{9}{2}\frac{9}{2}) \rightarrow \pi(4g\frac{7}{2}\frac{7}{2})$	0.563
	$\nu(4g\frac{9}{2}\frac{3}{2}) \rightarrow \pi(4g\frac{9}{2}\frac{1}{2})$	2.722	$\nu(4g\frac{9}{2}\frac{7}{2}) \rightarrow \pi(4g\frac{7}{2}\frac{7}{2})$	0.400	$\nu(3f\frac{5}{2}\frac{1}{2}) \rightarrow \pi(3f\frac{7}{2}\frac{3}{2})$	1.703
	$\nu(5h\frac{11}{2}\frac{11}{2}) \rightarrow \pi(5h\frac{11}{2}\frac{11}{2})$	1.321			$\nu(3f\frac{7}{2}\frac{3}{2}) \rightarrow \pi(3f\frac{5}{2}\frac{1}{2})$	0.266
¹¹⁰ Pd	$\nu(4g\frac{7}{2}\frac{5}{2}) \rightarrow \pi(4g\frac{9}{2}\frac{5}{2})$	2.554	$\nu(4g\frac{9}{2}\frac{5}{2}) \rightarrow \pi(4g\frac{7}{2}\frac{5}{2})$	1.028	$\nu(4g\frac{9}{2}\frac{7}{2}) \rightarrow \pi(4g\frac{7}{2}\frac{5}{2})$	1.570
	$\nu(4g\frac{7}{2}\frac{5}{2}) \rightarrow \pi(4g\frac{9}{2}\frac{3}{2})$	1.080	$\nu(4d\frac{3}{2}\frac{1}{2}) \rightarrow \pi(4d\frac{3}{2}\frac{1}{2})$	1.171	$\nu(3f\frac{5}{2}\frac{3}{2}) \rightarrow \pi(3f\frac{7}{2}\frac{1}{2})$	0.294
	$\nu(4g\frac{9}{2}\frac{5}{2}) \rightarrow \pi(4g\frac{9}{2}\frac{7}{2})$	2.705				
¹¹⁶ Cd	$\nu(4g\frac{7}{2}\frac{5}{2}) \rightarrow \pi(4g\frac{7}{2}\frac{7}{2})$	1.668	$\nu(4g\frac{9}{2}\frac{5}{2}) \rightarrow \pi(4g\frac{7}{2}\frac{7}{2})$	0.769	$\nu(3f\frac{7}{2}\frac{3}{2}) \rightarrow \pi(3f\frac{5}{2}\frac{1}{2})$	1.121
	$\nu(4d\frac{5}{2}\frac{1}{2}) \rightarrow \pi(4d\frac{3}{2}\frac{3}{2})$	0.462	$\nu(4g\frac{7}{2}\frac{7}{2}) \rightarrow \pi(4g\frac{9}{2}\frac{5}{2})$	0.927	$\nu(3f\frac{5}{2}\frac{3}{2}) \rightarrow \pi(3f\frac{7}{2}\frac{1}{2})$	2.647
			$\nu(4g\frac{7}{2}\frac{3}{2}) \rightarrow \pi(4g\frac{9}{2}\frac{1}{2})$	1.247	$\nu(3f\frac{7}{2}\frac{3}{2}) \rightarrow \pi(3f\frac{5}{2}\frac{3}{2})$	1.971
¹²⁸ Te	$\nu(4g\frac{7}{2}\frac{1}{2}) \rightarrow \pi(4g\frac{7}{2}\frac{3}{2})$	0.446	$\nu(4g\frac{9}{2}\frac{5}{2}) \rightarrow \pi(4g\frac{7}{2}\frac{3}{2})$	0.467	$\nu(4g\frac{9}{2}\frac{5}{2}) \rightarrow \pi(4g\frac{7}{2}\frac{7}{2})$	12.483
	$\nu(4g\frac{7}{2}\frac{3}{2}) \rightarrow \pi(4g\frac{9}{2}\frac{5}{2})$	0.380	$\nu(4g\frac{9}{2}\frac{3}{2}) \rightarrow \pi(4g\frac{7}{2}\frac{1}{2})$	0.198	$\nu(4d\frac{5}{2}\frac{3}{2}) \rightarrow \pi(4d\frac{3}{2}\frac{3}{2})$	7.316
¹³⁰ Te	$\nu(4g\frac{7}{2}\frac{5}{2}) \rightarrow \pi(4g\frac{7}{2}\frac{7}{2})$	0.462	$\nu(5h\frac{11}{2}\frac{1}{2}) \rightarrow \pi(5h\frac{9}{2}\frac{3}{2})$	0.430	$\nu(4g\frac{9}{2}\frac{5}{2}) \rightarrow \pi(4g\frac{7}{2}\frac{7}{2})$	2.543
	$\nu(4d\frac{3}{2}\frac{1}{2}) \rightarrow \pi(4d\frac{5}{2}\frac{3}{2})$	0.342	$\nu(4g\frac{9}{2}\frac{3}{2}) \rightarrow \pi(4g\frac{7}{2}\frac{1}{2})$	0.291	$\nu(4d\frac{5}{2}\frac{3}{2}) \rightarrow \pi(4d\frac{3}{2}\frac{3}{2})$	19.205
¹³⁴ Xe	$\nu(5h\frac{11}{2}\frac{9}{2}) \rightarrow \pi(5h\frac{11}{2}\frac{11}{2})$	0.713	$\nu(4g\frac{7}{2}\frac{5}{2}) \rightarrow \pi(4g\frac{9}{2}\frac{5}{2})$	0.659	$\nu(4d\frac{5}{2}\frac{1}{2}) \rightarrow \pi(4d\frac{3}{2}\frac{1}{2})$	0.784
			$\nu(4d\frac{3}{2}\frac{1}{2}) \rightarrow \pi(4d\frac{3}{2}\frac{3}{2})$	0.625	$\nu(4g\frac{9}{2}\frac{7}{2}) \rightarrow \pi(4g\frac{9}{2}\frac{5}{2})$	21.050
¹³⁶ Xe	$\nu(4g\frac{7}{2}\frac{3}{2}) \rightarrow \pi(4g\frac{9}{2}\frac{5}{2})$	0.710	$\nu(4d\frac{3}{2}\frac{3}{2}) \rightarrow \pi(4g\frac{3}{2}\frac{1}{2})$	0.392	$\nu(4g\frac{9}{2}\frac{7}{2}) \rightarrow \pi(4g\frac{9}{2}\frac{5}{2})$	23.661
	$\nu(4d\frac{3}{2}\frac{3}{2}) \rightarrow \pi(4g\frac{5}{2}\frac{5}{2})$	0.321	$\nu(4d\frac{5}{2}\frac{1}{2}) \rightarrow \pi(4d\frac{3}{2}\frac{1}{2})$	0.709		

TABLE VI: The strengths carried by the pnQRPA states contributing to the first, second and third (if any) peaks from the upper panels of Figs.1-4, are listed. On the left side of these numbers, the 2qp configurations closest in energy to the corresponding pnQRPA states, are given. This is the dominant configuration of the chosen pn phonon state. The states Φ_{nlj}^{IM} (see Eq. (2.6) are specified by the quantum numbers (NljI) where N=2n+1. Also, the orbital angular momentum values 0,1,2,..are mentioned by the letters s,p,d,.., respectively.

Nucleus	1st peak		2nd peak		3rd peak	
	pnQRPA energy	Strength	pnQRPA energy	Strength	pnQRPA energy	Strength
^{48}Ca	6.633	1.155	7.959	0.519	10.326	0.700
					12.611	3.344
^{96}Zr	7.077	0.602	10.316	1.040	12.416	5.842
	7.367	0.467	11.633	2.473	13.125	2.212
			11.901	0.786		
^{100}Mo	5.625	0.428	9.282	1.456	11.678	0.702
	5.790	4.950			12.104	0.716
	6.452	1.005				
^{104}Ru	5.181	1.342	9.028	0.885	11.296	0.563
	5.444	2.722	9.224	0.400	11.670	1.703
	6.327	1.321			11.900	0.266
^{110}Pd	3.470	2.554	10.319	1.028	12.641	1.570
	5.053	1.080	11.067	1.171	12.792	0.294
	6.339	2.705				
^{116}Cd	2.359	1.668	6.042	0.769	13.236	1.121
	3.221	0.462	6.378	0.927	13.346	2.647
			7.083	1.247	13.407	1.971
^{128}Te	5.339	0.445	10.173	0.467	13.713	12.483
	6.880	0.380	10.401	0.198	14.048	7.316
^{130}Te	6.553	0.462	10.129	0.430	13.652	2.543
	7.965	0.342	10.351	0.291	14.107	19.205
^{134}Xe	4.188	0.713	7.403	0.659	12.217	0.784
			7.761	0.625	14.865	21.050
^{136}Xe	7.545	0.710	11.437	0.392	15.359	23.661
	7.902	0.321	12.424	0.709		

TABLE VII: The energies of the pnQRPA states which give the largest strength contributions to the peaks in Figs. 1-4, left panels. The carried strengths are also given.

Nucleus	1st peak		2nd peak		3rd peak	
	Transition	Strength	Transition	Strength	Transition	Strength
^{48}Ti	$\pi(3p_{\frac{1}{2}\frac{1}{2}}) \rightarrow \nu(3p_{\frac{3}{2}\frac{3}{2}})$	0.153	$\pi(3f_{\frac{7}{2}\frac{7}{2}}) \rightarrow \nu(3f_{\frac{5}{2}\frac{5}{2}})$	0.307	$\pi(3f_{\frac{7}{2}\frac{3}{2}}) \rightarrow \nu(3f_{\frac{5}{2}\frac{1}{2}})$	0.562
^{96}Mo	$\pi(4d_{\frac{5}{2}\frac{1}{2}}) \rightarrow \nu(4d_{\frac{3}{2}\frac{1}{2}})$	0.146	$\pi(4d_{\frac{5}{2}\frac{3}{2}}) \rightarrow \nu(4d_{\frac{5}{2}\frac{5}{2}})$	0.025		
^{100}Ru	$\pi(4d_{\frac{5}{2}\frac{5}{2}}) \rightarrow \nu(4g_{\frac{3}{2}\frac{3}{2}})$	0.405	$\pi(4g_{\frac{9}{2}\frac{9}{2}}) \rightarrow \nu(4g_{\frac{7}{2}\frac{7}{2}})$	0.509		
			$\pi(4g_{\frac{9}{2}\frac{7}{2}}) \rightarrow \nu(4g_{\frac{7}{2}\frac{5}{2}})$	0.362		
^{104}Pd	$\pi(4g_{\frac{9}{2}\frac{5}{2}}) \rightarrow \nu(4g_{\frac{7}{2}\frac{7}{2}})$	0.441	$\pi(4g_{\frac{9}{2}\frac{1}{2}}) \rightarrow \nu(4g_{\frac{9}{2}\frac{3}{2}})$	0.247	$\pi(4g_{\frac{7}{2}\frac{5}{2}}) \rightarrow \nu(4g_{\frac{9}{2}\frac{7}{2}})$	0.023
			$\pi(4d_{\frac{5}{2}\frac{1}{2}}) \rightarrow \nu(4d_{\frac{5}{2}\frac{3}{2}})$	0.110		
^{110}Cd	$\pi(4d_{\frac{3}{2}\frac{3}{2}}) \rightarrow \nu(4d_{\frac{5}{2}\frac{1}{2}})$	0.273	$\pi(4g_{\frac{9}{2}\frac{7}{2}}) \rightarrow \nu(4g_{\frac{7}{2}\frac{5}{2}})$	0.110	$\pi(4g_{\frac{7}{2}\frac{5}{2}}) \rightarrow \nu(4g_{\frac{9}{2}\frac{3}{2}})$	0.027
			$\pi(4d_{\frac{5}{2}\frac{3}{2}}) \rightarrow \nu(4d_{\frac{3}{2}\frac{3}{2}})$	0.325		
^{116}Sn	$\pi(4g_{\frac{7}{2}\frac{7}{2}}) \rightarrow \nu(4g_{\frac{7}{2}\frac{5}{2}})$	0.391	$\pi(5f_{\frac{7}{2}\frac{7}{2}}) \rightarrow \nu(5f_{\frac{5}{2}\frac{5}{2}})$	0.117	$\pi(4d_{\frac{5}{2}\frac{1}{2}}) \rightarrow \nu(4d_{\frac{5}{2}\frac{3}{2}})$	0.019
			$\pi(4g_{\frac{7}{2}\frac{7}{2}}) \rightarrow \nu(4g_{\frac{9}{2}\frac{5}{2}})$	0.927		
^{128}Xe	$\pi(4d_{\frac{5}{2}\frac{1}{2}}) \rightarrow \nu(4d_{\frac{3}{2}\frac{3}{2}})$	0.011	$\pi(4g_{\frac{9}{2}\frac{5}{2}}) \rightarrow \nu(4g_{\frac{7}{2}\frac{5}{2}})$	0.020		
	$\pi(5h_{\frac{11}{2}\frac{1}{2}}) \rightarrow \nu(5h_{\frac{11}{2}\frac{3}{2}})$	0.011	$\pi(4g_{\frac{9}{2}\frac{7}{2}}) \rightarrow \nu(4g_{\frac{7}{2}\frac{7}{2}})$	0.041		
^{130}Xe	$\pi(4d_{\frac{5}{2}\frac{3}{2}}) \rightarrow \nu(4d_{\frac{3}{2}\frac{3}{2}})$	0.020	$\pi(4g_{\frac{9}{2}\frac{7}{2}}) \rightarrow \nu(4g_{\frac{7}{2}\frac{7}{2}})$	0.026		
	$\pi(5h_{\frac{11}{2}\frac{1}{2}}) \rightarrow \nu(5h_{\frac{11}{2}\frac{3}{2}})$	0.028				
^{134}Ba	$\pi(5f_{\frac{7}{2}\frac{7}{2}}) \rightarrow \nu(5f_{\frac{5}{2}\frac{5}{2}})$	0.106				
	$\pi(4g_{\frac{9}{2}\frac{3}{2}}) \rightarrow \nu(4g_{\frac{9}{2}\frac{1}{2}})$	0.086				
^{136}Ba	$\pi(4g_{\frac{9}{2}\frac{5}{2}}) \rightarrow \nu(4g_{\frac{7}{2}\frac{3}{2}})$	0.120				
	$\pi(4g_{\frac{9}{2}\frac{3}{2}}) \rightarrow \nu(4g_{\frac{7}{2}\frac{1}{2}})$	0.124				

TABLE VIII: The same as in Table VI but for the right panels of Figs. 1-4.

Nucleus	1st peak		2nd peak		3rd peak	
	pnQRPA energy	Strength	pnQRPA energy	Strength	pnQRPA energy	Strength
^{48}Ti	5.957	0.153	6.940	0.307	7.565	0.562
^{96}Mo	3.361	0.146	4.224	0.025		
^{100}Ru	2.099	0.405	3.617	0.509		
			4.437	0.362		
^{104}Pd	0.863	0.441	4.265	0.247	10.725	0.023
			5.300	0.110		
^{110}Cd	1.817	0.273	4.405	0.110	6.873	0.027
			4.531	0.325		
^{116}Sn	1.727	0.391	5.718	0.117	8.461	0.019
			6.378	0.927		
^{128}Xe	2.554	0.011	5.025	0.041		
	3.246	0.011	5.479	0.020		
^{130}Xe	3.356	0.020	4.674	0.026		
	3.446	0.028				
^{134}Ba	3.756	0.106				
	3.803	0.086				
^{136}Ba	3.242	0.120				
	3.534	0.124				

TABLE IX: The same as in Table VII, but for the right panels of Figs. 1-4.

Nucleus	^{48}Sc	^{96}Nb	^{100}Tc	^{104}Rh	^{110}Ag	^{116}In	^{128}I	^{130}I	^{134}Cs	^{136}Cs
$E_{1^+}[\text{keV}]$	338	1116	0	0	0	0	58	85	177	177

TABLE X: The experimental energies for the first 1^+ states in the intermediate odd-odd nuclei are given in units of keV. Data are taken from Refs.[41, 42, 43, 44, 45, 46, 47, 48, 49, 50]. The states in ^{48}Sc and ^{96}Nb , at 338 and 1116 keV respectively, are not assigned with angular momentum and parity. Here we, ad hoc, suppose that they have the angular momentum equal to one and a positive parity. For ^{136}Cs , there is no available data for energy levels. For this case we adopted the same excitation energy for the state 1^+ as in ^{134}Cs . Also for $^{128,130}\text{I}$ the energies for 1^+ are the same as in Ref.[51]

Nucleus	SSD		present	
	M_{GT}	$t_{1/2}$	M_{GT}	$t_{1/2}$
^{100}Mo	0.211	$5.860 \cdot 10^{-19}$	0.305	$2.82 \cdot 10^{-19}$
^{104}Ru	0.616	$7.493 \cdot 10^{-21}$	0.781	$4.655 \cdot 10^{-21}$
^{110}Pd	0.551	$2.208 \cdot 10^{-20}$	0.263	$9.694 \cdot 10^{-20}$
^{116}Cd	0.421	$1.780 \cdot 10^{-19}$	0.116	$23.63 \cdot 10^{-19}$
^{128}Te	0.032	$26.950 \cdot 10^{-24}$	0.090	$3.38 \cdot 10^{-24}$

TABLE XI: The M_{GT} and $t_{1/2}$ values obtained with the single state dominance (*SSD*) hypothesis. For an easy comparison we give also the values obtained within the present formalism. By contrast to the $t_{1/2}$ values given in Table IV, here the half lives correspond to $g_A = 1$.

Before closing this Section we would like to say a few more words about the adopted procedure for fixing the dipole proton-neutron strength parameters. For the sake of a unitary treatment, the half lives of all double beta decaying nuclei were calculated by taking for g_A the value 1.254. However, in five of the situations considered the single beta properties for the intermediate odd-odd nuclei are determined by supposing an effective value ($g_A=1.$) for the axial-vector coupling strength, which might simulate the contribution of the higher energy states. Thus, although the nuclear matrix elements as well as the proton-neutron interaction strengths are similar for double and single transitions, we considered that the two sets of properties mentioned above are influenced by different parts of the proton-neutron QRPA excitation spectrum. In this context it is worth mentioning that some time ago Abad *et al.* [64] advanced the single state dominance hypothesis (SSDH) which asserts that for double beta decay processes where the intermediate odd-odd nucleus has the state 1^+ as ground state, most of the contribution to the double beta matrix element comes from the first intermediate dipole state. If that hypothesis works, then the double beta process is dominated by two virtual and successive single β^- transitions, one from the ground state of the mother nucleus to the ground state of the intermediate odd-odd nucleus, while the other one from there to the ground state of the daughter nucleus. In the meantime the SSDH has been considered by many authors [65, 68, 69, 70, 71, 72, 73, 74]. As shown in Table X, four odd-odd isotopes have indeed the first 1^+ as ground state. Moreover, there are also available data for β^- and β^+/EC transitions of ^{130}I . Therefore, for all five isotopes from Table II we checked the SSDH validity by keeping in Eq. (2.21) only the first term from the sum and considering the states overlap equal to unity. Also the $t_{1/2}$ values are calculated by considering $g_A = 1$. The results are compared with those obtained by summing up over all pnQRPA states, otherwise keeping $g_A = 1$ in order to have a fair comparison. Results are listed in Table XI. From there one may conclude that indeed our calculations confirm the SSDH for ^{100}Mo , ^{104}Ru and ^{110}Pd , but not for the remaining two double beta nuclei, ^{116}Cd and ^{128}Te . Most likely for these cases the summation in the expression of M_{GT} should be extended from one to few states.

It is worthwhile to address the question how stable are these results against changing the dimension of the single particle basis. We checked this feature with a positive result. To be more concrete let us describe the modifications obtained for ^{110}Pd . For this isotope we increased the dimension D_1 from 23 to 27, otherwise keeping the same parameters for

single particle states as before. We changed the pairing strengths in order to preserve the pairing properties, i.e. to have the gap parameters unchanged. The new (G_p, G_n) for mother and daughter are $(0.281, 0.271)$ MeV and $(0.2795, 0.1665)$ MeV, respectively. The pnQRPA matrix has the dimension $D_2 = 186$. The ISR value deviates from $N - Z$ by 3%. The proton-neutron interaction strengths have been changed to $(\chi, g_{pp}) = (0.13735, 2.4)$ MeV in order to keep the $\log ft$ values for the single beta transitions of ^{110}Ag close to the experimental data. The results for these observables are 4.84 for β^- and 3.70 for β^+/EC . The double beta transition amplitude and the $T_{1/2}$ obtained under the new circumstances, are 0.2626 and $15.881 \cdot 10^{19} \text{yr}$. One notes that these values are very close to those listed in Table IV. One may conclude that the results are stable against enlarging the single particle space and moreover our choice for D_1 is motivated by the fact that ISR is satisfied.

IV. CONCLUSIONS

In the previous sections we completed the project started in Ref.[15] by studying the $2\nu\beta\beta$ decay of another ten even-even nuclei exhibiting various shapes. In the chosen cases the mother and daughter nuclei have the following shapes: a) both are spherical, b) both deformed-prolate, c) both deformed-oblate, d) one spherical and another deformed-prolate, e) both are near spherical but prolate, f) both are near spherical but oblate. The deformations obtained for the ten isotopes are similar to those of Ref.[57, 59]. In some cases these are different from nuclear deformations reported in Ref.[60]. Indeed, for example in the present paper as well as in Ref.[57], the quadrupole deformation for ^{100}Mo is negative while in Ref.[60] this is positive. Moreover, as shown in Ref.[60] a negative deformation is reached in ^{106}Mo . The reason for this discrepancy might be the fact that there the stationary points of the energy function are obtained in the space of quadrupole and hexadecapole deformations while here only the quadrupole variable is considered. Moreover, here an angular momentum projected single particle basis is used.

It is manifest the fact that an oblate to oblate single beta transition is involving single particle configurations which are different from those appearing in a prolate to prolate transition. Indeed, suppose that a certain number of nucleons are distributed alternatively in a prolate and an oblate single particle levels and that in the first case the Fermi level for neutrons is characterized by a small quantum number I . In this case the β^- strength for the

prolate to prolate transition is carried by single particle dipole transitions between states of low I as well as of large I but originating from the upper shell. By contrary, in the oblate to oblate transitions, the privileged transitions are those relating neutron and proton single particle states with large I and those of small I from the upper shell. Such cases can be easily identified in Tables VI and VIII. Due to the feature mentioned above the strength fragmentation is expected to be more pronounced in the oblate to oblate transitions. Actually such a situation is met for ^{100}Mo , ^{104}Ru , ^{110}Pd and ^{116}Cd .

The structure of the peaks seen in Figs 1,2 in the β^- strength distribution of the nuclei mentioned before is as follows. In ^{100}Mo the peaks are determined by transitions inside the shells 1g (1st peak) 2d (2nd peak) and 1g and 1f (3rd peak). For ^{104}Ru the first two peaks are determined mainly by the transitions from the shell 1g while the third one by the transition from the shell 1f. In ^{110}Pd the following shells are involved in the transitions contributing most to the three peaks: 1g (1st peak), 1g, 2d (2nd peak) and 1g, 1f (3rd peak). For ^{116}Cd only one shell contributes most to any of the three dominant peaks: 1g (1st and 2nd peaks), 1f (3rd peak).

Note that for Te and Xe isotopes, the β^- strength is mainly concentrated in one pnQRPA state. These nuclei are almost spherical (Te isotopes are soft prolate while Xe isotopes are soft oblate). Moreover, in the daughter nuclei the nuclear deformation has the same sign as in the corresponding mother nuclei. In ^{128}Te and ^{130}Te the dominant single particle state np transitions are $\nu(4g_{\frac{9}{2}\frac{5}{2}}) \rightarrow \pi(4g_{\frac{7}{2}\frac{7}{2}})$ and $\nu(4d_{\frac{5}{2}\frac{3}{2}}) \rightarrow \pi(4d_{\frac{3}{2}\frac{3}{2}})$, respectively. In Xe isotopes the np single particle transition $\nu(4g_{\frac{9}{2}\frac{7}{2}}) \rightarrow \pi(4g_{\frac{9}{2}\frac{5}{2}})$, prevails.

The transition amplitudes M_{GT} and half lives for the $2\nu\beta\beta$ process were calculated within the pnQRPA approach by using a projected spherical basis. The agreement with the available data is quite good. The adopted fitting procedure for the pn dipole interaction strengths yield large values for g_{pp} , in several cases. These values are not far from the critical value, where the pnQRPA breaks down. It is an open question whether for these transitions a good agreement with the data would be possible by keeping a small g_{pp} , but accounting for higher pnQRPA effects. Inspecting the Table IV, one can judge not only on the agreement of the present results with the experimental data but also on the comparison between predictions of different theoretical approaches. Indeed, the agreement with experimental data is reasonably good. Although they are based on different formalisms as well as different single particle states the present results and those of Suhonen *et al.*[1, 34, 35] are not far

from each other. Comparing the results of the present paper, obtained with χ and g_{pp} given by Eq.(3.2) and the corresponding predictions from Refs.[36, 37, 39], one notices that they are quite different.

It is worth mentioning that for ^{104}Ru and ^{110}Pd the pn dipole interactions are fully determined by fitting the data concerning the β^+/EC and β^- decay $\log ft$ values of the ground state (1^+) of the intermediate nuclei ^{104}Rh and ^{110}Ag , respectively. The predictions for the double beta emitter half lives are $0.76 \cdot 10^{21}\text{yr}$ and $15.85 \cdot 10^{19}\text{yr}$. They are 40 and 8 times smaller than the corresponding predictions of Ref.[37]. Our prediction for the half-life of ^{134}Xe , against double beta decay, is $3.75 \cdot 10^{24}\text{yr}$ which exceeds by a factor 15 the corresponding finding of Ref.[36, 58].

The single state dominance is confirmed, by our formalism, to be valid for ^{100}Mo , ^{104}Ru and ^{110}Pd .

Finally we may conclude that the projected spherical single particle basis provides a suitable framework for a unified description of the double beta properties of spherical and deformed nuclei. The results presented in the previous publication [15] and here constitute a good starting point for studying the higher pnQRPA contributions to the $2\nu\beta\beta$ process as well as the transitions populating the daughter nuclei in an excited state.

-
- [1] J. Suhonen and O. Civitarese, Phys.Rep. **300** (1998) 123.
 - [2] J.D. Vergados, Phys. Rep. **361** (2001) 1.
 - [3] H. Primakof and S. Rosen, Rep. Prog. Phys. **22** (1959) 125.
 - [4] W. C. Haxton and G. J. Stephenson, Jr. Prog. Part. Nucl. Phys. **12**(1984) 409.
 - [5] T. Tomoda, Re. Prog. Phys. **54** (1991) 53.
 - [6] A. Faessler, Prog. Part. Nucl. Phys. **21** (1988) 183.
 - [7] H. V. Klapdor-Kleingrothaus, *Sixty Years of Double Beta Decay*, World Scientific, Singapore (2001).
 - [8] A. A. Raduta, Prog. Part. Nucl. Phys. **48**(2002) 233.
 - [9] A. A. Raduta, A. Faessler and D.S. Delion, Nucl. Phys. **A 564** (1993) 185; Phys. Lett.**B 312** (1993) 13.
 - [10] A. A. Raduta, D. S. Delion and A. Faessler, Nucl. Phys. **A 617** (1997) 176.

- [11] H. Homma, E. Bender, M. Hirsch, K. Muto, H.V. Klapdor-Kleingrothaus and T. Oda, Phys. Rev. **C54** (1996) 2972.
- [12] P.Sarriguren, E. Moya de Guerra, A. Escuderos, A. C. Carrizo, Nucl. Phys. **A 635** (1998) 55; P. Sarriguren, E. Moya de Guerra and A. Escuderos, Nucl. Phys. **A658** (1999)13; Nucl. Phys. **A 691** (2001) 631; Phys. Rev. **C 64**(2001) 064306; P. Sarriguren,E. Moya de Guerra, L. Pacearescu, A. Faessler, F. Simkovic and A. A. Raduta, Phys. Rev. **C 67** (2003) 044313.
- [13] J. Engel, M. Bender, J. Dobaczewski, W. Nazarewicz and R. Surnam, Phys. Rev. **C 60** (1999) 014302; M. Bender, J. Dobaczewski, J. Engel and W. Nazarewicz, Phys. Rev. **C 65** (2002) 054322.
- [14] F. Simkovic, L. Pacearescu and A. Faessler, Nucl. Phys. **A 733** (2004) 321.
- [15] A. A. Raduta, A. Escuderos, A. Faessler, E. Moya de Guerra and P. Sarriguren, Phys. Rev. **C69**(2004) 064321.
- [16] A. A. Raduta, D. S. Delion and N. Lo Iudice, Nucl. Phys. **A 564** (1993) 185.
- [17] A. A. Raduta, N. Lo Iudice and I. I. Ursu, Nucl. Phys. **A584** (1995) 84.
- [18] A. A. Raduta, Al. H. Raduta and Ad. R. Raduta, Phys. Rev. **B 59** (1999) 8209;A. A. Raduta, E. Garrido and E. Moya de Guerra, Eur. Phys. Jour. **D 15** (2001) 65
- [19] A. A. Raduta, A. Escuderos and E. Moya de Guerra, Phys. Rev. **C 65** (2002) 024312.
- [20] S.G.Nilsson,Mat.Fys.Medd. K. Dan. Vid.Selsk.**29** no. 16 (1955).
- [21] A.A.Raduta, A.Faessler and S.Stoica, Nucl. Phys. **A534** (1991) 149.
- [22] M. E. Rose, Elementary Theory of Angular Momentum (Wiley, New York, 1957).
- [23] P.Ring and P.Shuck, The Nuclear Many-Body Problem, Springer,1980,p. 76.
- [24] S.R. Elliot and P. Vogel, Ann. Rev. Nucl. Part. Sci. **52** (2002) 115.
- [25] A. S. Barabash, Czech. J. Phys. **52**(2002) 567.
- [26] P. Moller and J. Randrup, Nucl. Phys **A 514** (1990) 1.
- [27] E. Bender, K. Muto and H. V. Klapdor, Phys. Lett. **B208** (1988) 53.
- [28] K. Grotz and H. V. Klapdor, Nucl. Phys. **A460** (1986) 395
- [29] H. Ejiri et al., Phys. Lett. **B258** (1991) 17.
- [30] T. Kirsten, E. Heusser, D. Kaether, J. Oehm, E. Pernicka, H. Richter, Proceedings of the International Symposium on Nuclear Beta Decays and Neutrino, T.Kotani, H. Ejiri, E. Takasugi(eds.),p.81. Singapore:World Scientific 1986;
- [31] S. I. Vasil'ev, A. A. Klimenko, S. B. Osetrov, A. A. Pomansky and K. A. Smol'nikov, JETP

- Lett. **51** (1990) 622.
- [32] E.W.Hennecke, O.K. Manuel and D.D.Sabu, Phys. Rev. **C11** (1975) 1378.
- [33] W.J.Lin et al., Nucl. Phys. **A481** (1988) 477.
- [34] J. Suhonen and O. Civitarese, Phys. Rev. **C 49** (1994) 3055.
- [35] M. Aunola, J. Suhonen, Nucl. Phys. **A602** (1996) 133.
- [36] K. Grotz and H. V. Klapdor, Phys. Lett. **157 B**(1985) 242.
- [37] M. Hirsch, X. R. Wu, H. V. Klapdor-Kleingrothaus, Ching Cheng-rui, Ho Tso-hsiu, Physics Reports **242** (1994) 403.
- [38] H. V. Klapdor and K. Grotz, Phys. Lett. **142 B** (1984) 323.
- [39] L. Zhao, B. A. Brown, W. A. Richter, Phys. Rev. **C 42** (1990) 1120.
- [40] A. Balysch et al., Phys. Lett. **B 356**1995.
- [41] T.W.Burrow, Nuclear Data Sheets **68** (1993) 1.
- [42] L.K.Pekev, Nuclear Data Sheets **68** (1993) 165.
- [43] Balraj Singh, Nuclear Data Sheets **81** (1997) 1.
- [44] Jean Bachot, Nuclear Data Sheets **64** (1991) 1.
- [45] D. De Frenne and E. Jacobs, Nuclear Data Sheets **89** (2000) 481.
- [46] Jean Bachot, Nuclear Data Sheets **92** (2001) 455.
- [47] M, Kanbe, K. Kitao, Nuclear Data Sheets **94** (2001) 227.
- [48] Balraj Singh, Nuclear Data Sheets **93** (2001) 33.
- [49] Yu. V. Sergeenkov, Nuclear Data Sheets **71** (1994) 557.
- [50] A. A. Sonzogni, Nuclear Data Sheets**95** (2002) 837.
- [51] R. Madey, B.S.Flanders, B.D. Anderson, A. R. Baldwin, J.W. Watson, S.M. Austin, C.C.Foster,H.V.Klapdor and K. Grotz, Phys. Rev. **C40** (1989) 540.
- [52] H. Akimune, H. Ejiri, M. Fujiwara, I. Daito, T. Inomata, R. Hazama, A. Tamii, H. Toyokawa, M. Yosoi, Phys. Lett. **B394** (1997) 23.
- [53] H.V.Klapdor, Prog. Part. Nucl. Phys. **17** (1986) 419.
- [54] B. D. Anderson, T. Chittrakarn, A. R. Baldwin, C. Lebo, R. Madey, P. C. Tandy, J. W. Watson, B. A. Brown and C. C. Foster, Phys. Rev. **C31** (19985) 1161.
- [55] L. Zamick and N. Auerbach, Phys. Rev. **C 26** (1982) 2185.
- [56] D. Cha, Phys. Rev. **C27** (1987) 2269.
- [57] K. Grotz and H. V. Klapdor, Nucl. Phys. **A 460** (1986) 395.

- [58] X.R. Wu, M. Hirsch, A. Staudt, H.V. Klapdor-Kleingrothaus, Cheng-Rui Ching and Tso-Hsui Ho, *Commun. Theor. Phys.* **20** (1993) 453.
- [59] G. Audi and A.H. Wapstra, *Nucl. Phys.* **A595** (1995) 409; G. Audi, O. Bersillon, J. Blachot and A. H. Wapstra, *Nucl. Phys.* **A 624** (1997) 1.
- [60] G. A. Lalazissis, S. Raman and P. Ring, *At. Data and Nucl. Data Tables* **60** (1995) 177.
- [61] K. Ikeda, *Prog. Theor. Phys.* **31** (1964) 434; K. Ikeda, S. Fujita and J. I. Fujita, *Phys. Lett.* **3** (1963) 271; J. I. Fujita and K. Ikeda, *Prog. Theor. Phys.* **36** (1966) 288.
- [62] D. Zheng, L. Zamick, N. Auerbach, *Ann. Phys.* **197** (1990) 343.
- [63] E. Caurier, A. Poves, A. P. Zuker, *Phys. Lett.* **B 252** (1990) 13.
- [64] J. Abad, A. Morales, R. Nunes-Lagosadn A. F. Pacheco, *Ann. Fis. A* 80 (1984) 9.
- [65] A. Garcia *et al.*, *Phys. Rev.* **C 47** (1993) 2910.
- [66] M. Bhattacharya, A. Garcia, M. Hindi, E. Norman, C. Ortiz, N. Kaloskamis, C. Davids, O. Civitarese, J. Suhonen, *Phys. Rev.* **C58** (1998) 1247.
- [67] H. Miyahara *et al.*, *Nucl. Instrum. Methods, Phys. Res.* **a 353** (1995) 229; C. M. Lederer and V. S. Shirley, *Table of Isotopes*, seventh edition, John Wiley and Sons, INC., p. 631.
- [68] H. Ejiri, *Nucl. Phys. A* 577 (1994) 399c.
- [69] O. Civitarese and J. Suhonen, *Phys. Rev. C* 58 (1998) 1535.
- [70] O. Civitarese and J. Suhonen, *Nucl Phys.* **A653** (1998) 321.
- [71] F. Simkovic, P. Domin and S. V. Semenov, *J. Phys. G: Nucl. Part. Phys.* **27** (2001) 2233.
- [72] H. Ejiri, *Prog. in Part. and Nucl. Phys.* **48** (2002) 185.
- [73] O. Civitarese, J. Suhonen, H. Ejiri, *Eur. Phys. J.* **A 16** (2003) 353.
- [74] P. Domin, S. Kovalenko, F. Simkovic and S. V. Semenov, arXiv: nucl-th/0411002 v1.

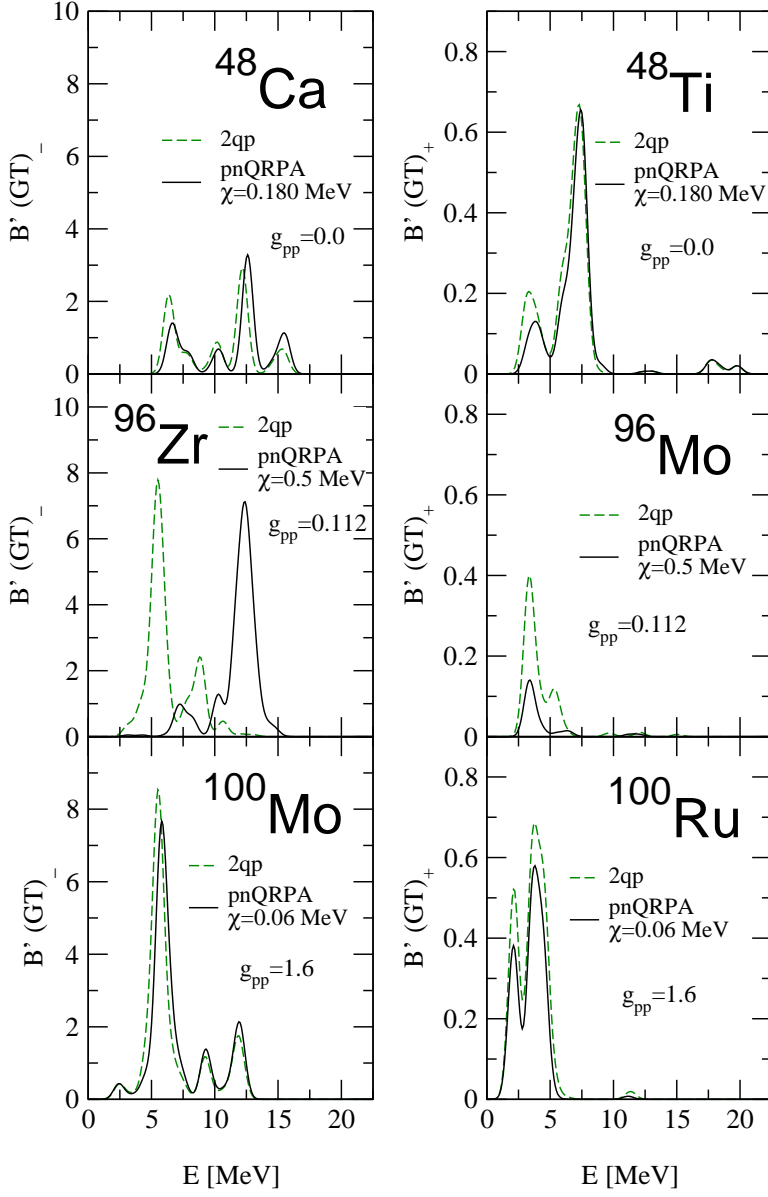


FIG. 1: (Color on line) Single β^- strength, for ^{48}Ca (upper-left panel), ^{96}Zr (middle-left panel), ^{100}Mo (bottom-left panel), and single β^+ strength for ^{48}Ti (upper-right panel), ^{96}Mo (middle-right panel), ^{100}Ru (bottom-right panel), folded with a Gaussian function having the width of 1 MeV, are plotted as a function of the energy within the BCS and pnQRPA approximation. The pnQRPA calculations correspond to the values of χ and g_{pp} listed inside the graphs.

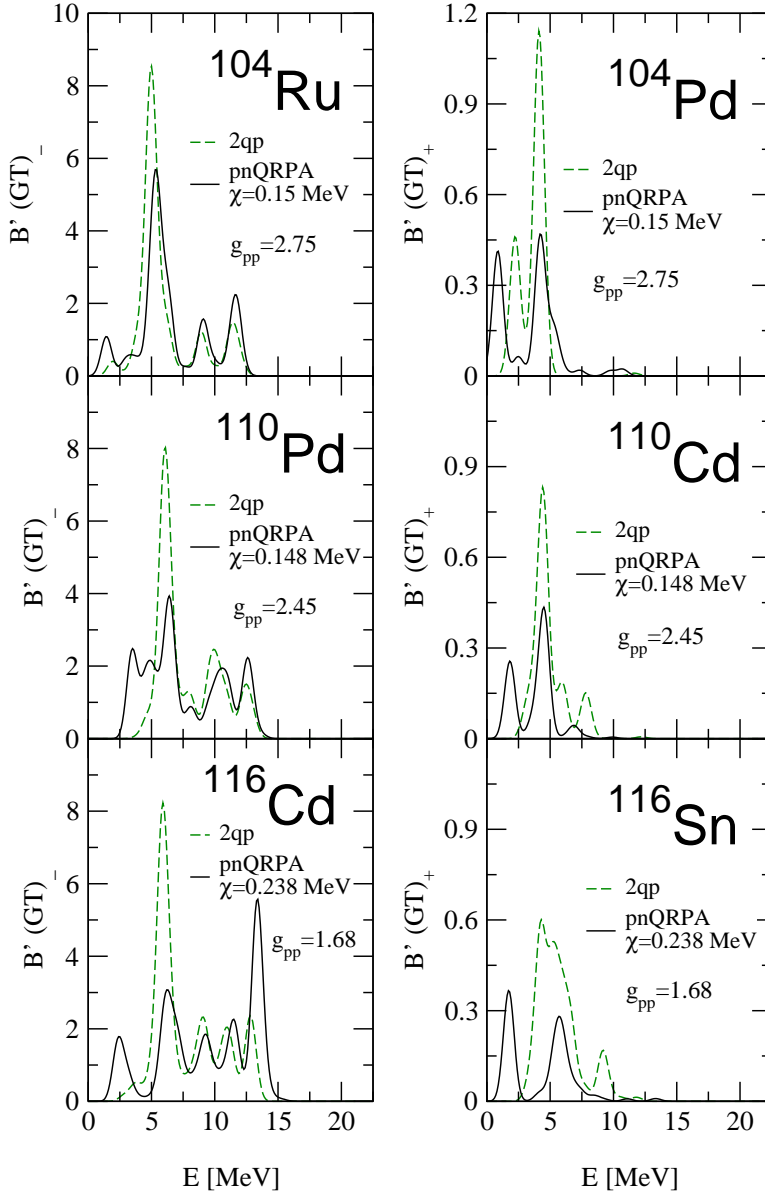


FIG. 2: (Color on line) Single β^- strength, for ^{104}Ru (upper-left panel), ^{110}Pd (middle-left panel), ^{116}Cd (bottom-left panel), and single β^+ strength for ^{104}Pd (upper-right panel), ^{110}Cd (middle-right panel), ^{116}Sn (bottom-right panel), folded with a Gaussian function having the width of 1 MeV, are plotted as a function of the energy within the BCS and pnQRPA approximation. The pnQRPA calculations correspond to the values of χ and g_{pp} listed inside the graphs .

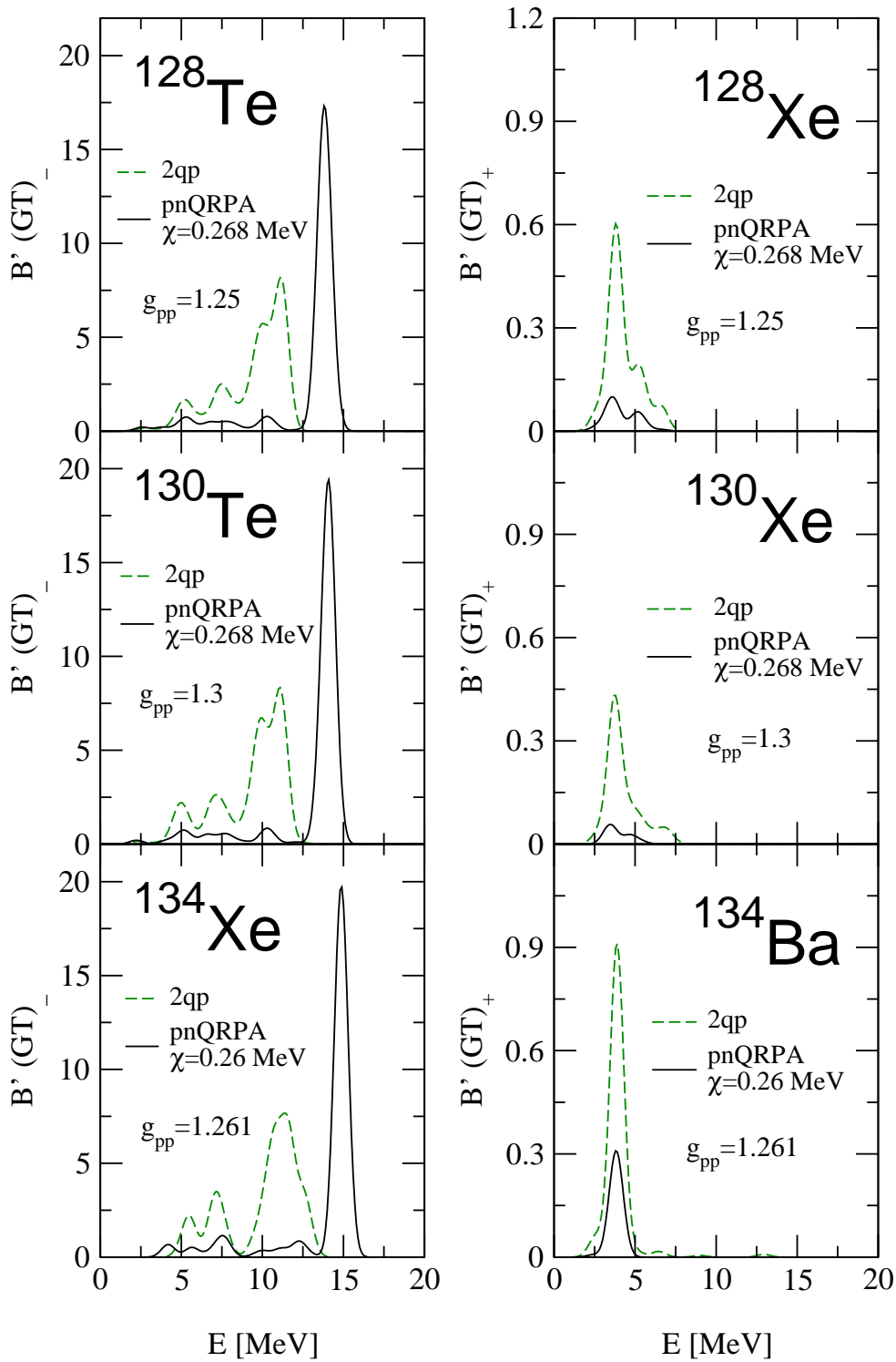


FIG. 3: (Color on line) Single β^- strength, for ^{128}Te (upper-left panel), ^{130}Te (middle-left panel), ^{134}Xe (bottom-left panel), and single β^+ strength for ^{128}Xe (upper-right panel), ^{130}Xe (middle-right panel), ^{134}Ba (bottom-right panel), folded with a Gaussian function having the width of 1 MeV, are plotted as a function of the energy within the BCS and pnQRPA approximation. The pnQRPA calculations correspond to the values of χ and g_{pp} listed inside the graphs .

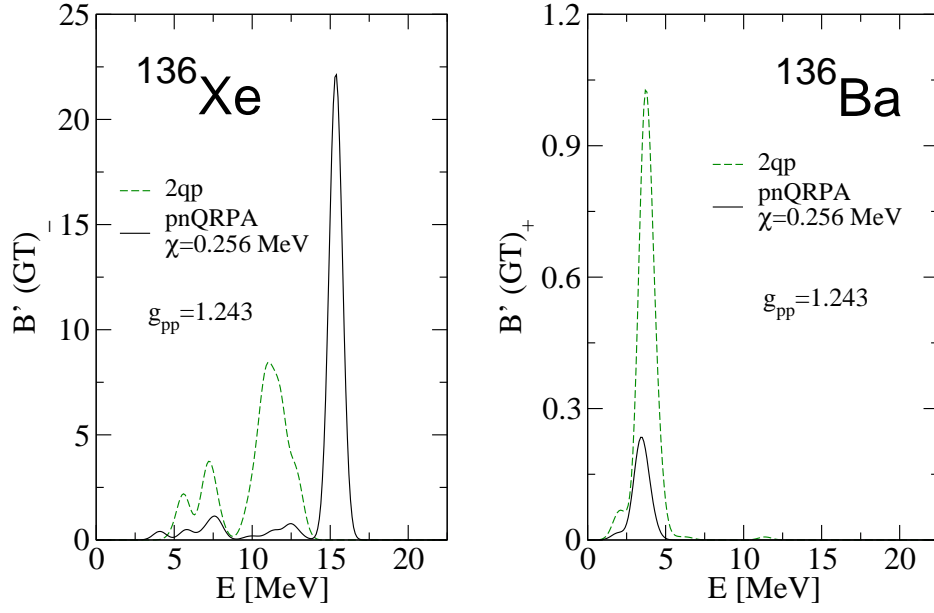


FIG. 4: (Color on line) Single β^- strength, for ^{136}Xe (left panel), and single β^+ strength for ^{136}Ba (right panel), folded with a Gaussian function having the width of 1 MeV, are plotted as a function of the energy within the BCS and pnQRPA approximation. The pnQRPA calculations correspond to the values of χ and g_{pp} listed inside the graphs.

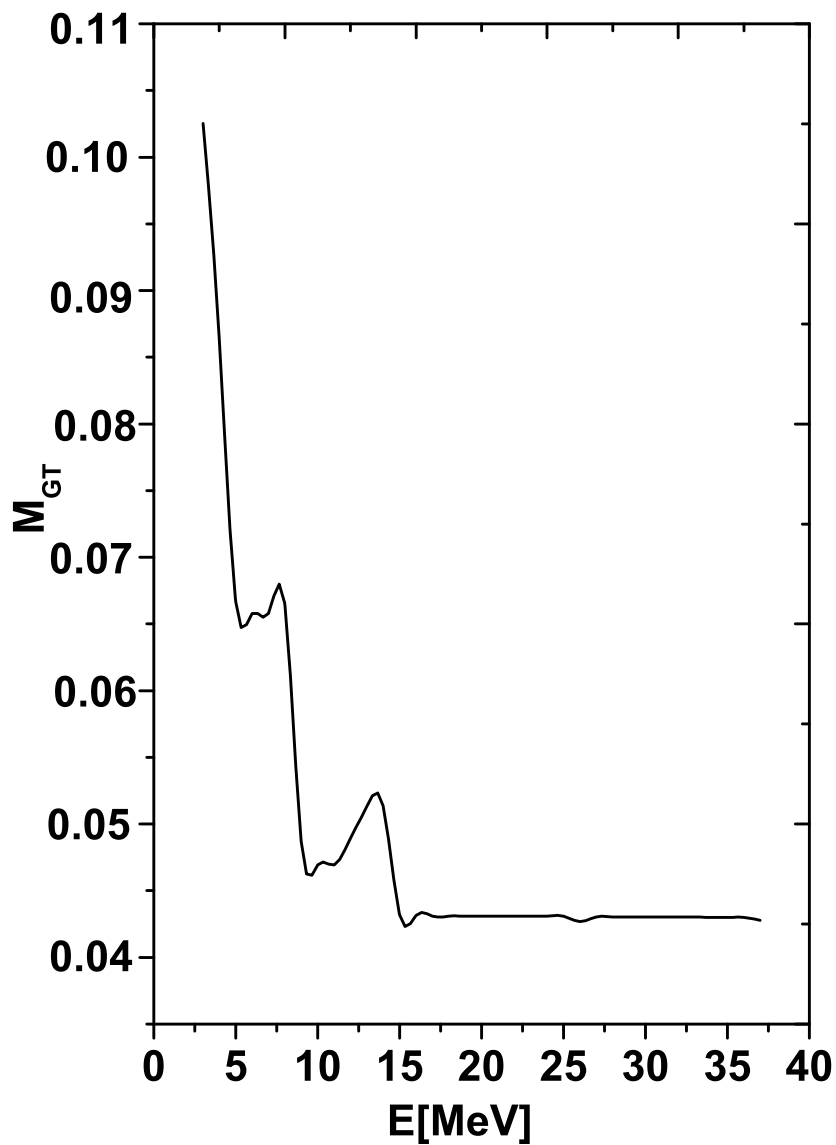


FIG. 5: Double beta transition amplitude M_{GT} , given by Eq.(2.21), is represented as function of energy E for ^{48}Ca . The summation over k , in EQ. (2.21), is restricted by $E_k \leq E$ where E_k is defined by Eq. (2.22).